PM

Formation of Functional Polyetheylenimine-Based Nanogels for Tumor MR Imaging and Chemotherapy

MASTER'S DEGREE PROJECT

Yu Zou

MASTER IN NANOCHEMISTRY AND NANOMATERIALS

UNIVERSIDADE da MADEIRA

A Nossa Universidade

www.uma.pt

July | 2019

Formation of Functional Polyetheylenimine-Based Nanogels for Tumor MR Imaging and Chemotherapy

MASTER'S DEGREE PROJECT

Yu Zou
MASTER IN NANOCHEMISTRY AND NANOMATERIALS

ORIENTATION
Xiangyang Shi

CO-ORIENTATION
Helena Maria Pires Gaspar Tomás

Formation of Functional Polyethylenimine-Based Nanogels for Tumor MR Imaging and Chemotherapy

Thesis submitted to the University of Madeira in order to obtain the degree of Master in Nanochemistry and Nanomaterials

by Yu Zou

Study performed under the supervision of Prof. Xiangyang Shi
and Prof. Helena Tomás

Centro de Química da Madeira,
Campus Universitário da Penteada, 9000-390 Funchal, Portugal

July 2019

DECLARATION

I hereby declare that this thesis is the result of my own work, is original and was written by me. I also declare that its reproduction and publication by the University of Madeira will not break any third-party rights and that I have not previously (in its entirety or in part) submitted it elsewhere for obtaining any qualification or degree. Furthermore, I certify that all the sources of information used in the thesis were properly cited.

Funchal, July 2019

ACKNOWLEDGEMENTS

The two-years of my master's life is a precious memory in my life. In these two years, I have not only gained the professional knowledge and scientific research attitude, but also the basic experimental skills. The research experience gave me courage and determination to face the difficulties. Since starting the Master degree, the selfless dedication of the teachers and the mutual help from other graduate students have made me feel the harmony and warmth all the time. I sincerely thank my supervisor Prof. Xiangyang Shi and co-supervisor Prof. Helena Tomás for all their help. In the past year, they gave great support to my work and let me get on the right way of scientific research. This thesis was completed under their careful guidance.

I want to present my gratitude to Dr. Wenjie Sun and Mr. Yu Fan. In the past two years, they have provided valuable advice and guidance on my study and work. When I faced trouble, they did their best to help me. I am glad that I have earned their friendship.

I am also grateful to Lydia and Sabriye, who led me to adapt to the life in Madeira. They are excellent friends and I learned a lot from them.

I would like to thank all members of the Centro de Química da Madeira (CQM) and Prof. Shi's group for the friendship and support, not only in the lab, but also in the meetings and gatherings.

I acknowledge the CQM (supported by FCT - *Fundação para a Ciência e a Tecnologia*, Project PEst-OE/QUI/UI0674/2019, Portuguese Government funds) and the University of Madeira for providing me with the possibility to perform my master project. ARDITI-*Agência Regional para o Desenvolvimento da Investigação Tecnologia e Inovação* is also acknowledged for the project M1420-01-0145-FEDER-000005-Centro de Química da Madeira - CQM^{+}(Madeira 14–20 Program).

This research would not be possible without the financial support of the Sino-German Center for Research Promotion (GZ1505), National Natural Science Foundation of China (81761148028), the Shanghai Education Commission through the Shanghai Leading Talents Program (ZX201903000002), and the Science and Technology Commission of Shanghai Municipality (19XD1400100, 17540712000 and 18520750400).

Work presentation in Scientific Meetings in the scope of the Master Project:

Yu Zou, Xiangyang Shi*. Incorporation of ultrasmall iron oxide nanoparticles and Doxorubicin within polymer nanogels for tumor theranostics. 11th International Dendrimer Symposium-IDS11, Funchal, Portugal, July 14-18, 2019 (poster presentation).

ABSTRACT

Nanogels (NGs) are three dimensional networks composed of hydrophilic or amphiphilic polymer chains, allowing for effective and homogeneous encapsulation of drugs, genes or imaging contrast agents for biomedical applications. Polyethylenimine (PEI), possessing sufficient positively charged amine groups, is an ideal platform for NG development. In this study, we synthesized PEI-based NGs loaded with both MR contrast agent ultrasmall iron oxide (Fe_3O_4) nanoparticles (NPs) and the anticancer drug doxorubicin (DOX) for tumor theranostics.

The synthesis of PEI-based NGs was first carried out by an inverse mini-emulsion (water-in-oil, W/O) crosslinking strategy. Secondly, the NGs were conjugated with ultrasmall Fe_3O_4 NPs which was performed via a hydrothermal method through 1-ethyl-3-(3-dimethylaminopropyl)carbodiimide hydrochloride (EDC) chemistry. Then the amine groups of the NGs were acetylated by acetic anhydride. The formed PEI-based NGs possess good dispersibility and cytocompatibility. The drug release profile was studied, as well as the impact of the environmental pH on the release rate of DOX. Results proved that the hybrid NGs facilitated a sustained release of DOX with a higher release rate under acidic pH. Furthermore, *in vitro* studies showed that Fe_3O_4/PEI-Ac NGs had no cytotoxicity towards 4T1 tumor cells, unlike Fe_3O_4/PEI-Ac NGs/DOX complexes and Free DOX. The PEI-based NGs presented significantly enhanced r_1 relaxivity of 2.29 $mM^{-1}s^{-1}$ when compared to free ultrasmall Fe_3O_4 NPs (1.15 $mM^{-1}s^{-1}$), as well as excellent drug loading efficiency (51.4%). Strikingly, the NGs presented enhanced T_1 MR imaging ability and a high therapeutic efficacy towards cancer cells *in vitro* and a xenografted tumor model *in vivo*.

Keywords: Polyetheylenimine; nanogels; ultrasmall iron oxide NPs; doxorubicin; theranostics

RESUMO

Os nanogéis (NGs) são redes tridimensionais compostas por cadeias poliméricas, hidrofílicas ou anfifílicas, que permitem o encapsulamento efetivo e homogéneo de fármacos, genes ou agentes de contraste para aplicações biomédicas. A polietilenimina (PEI), por possuir muitos grupos amina carregados positivamente, constitui uma plataforma ideal para o desenvolvimento de NGs. Neste estudo, sintetizaram-se NGs à base de PEI, nos quais se incorporaram nanopartículas de óxido de ferro (Fe_3O_4) e também o fármaco anticancerígeno doxorubicina (DOX) com vista ao tratamento e simultâneo diagnóstico de tumores.

Em primeiro lugar, a preparação dos NGs foi levada a cabo através de um processo de reticulação de mini-emulsão inversa (água em óleo). De seguida, os NGs foram conjugados com nanopartículas de Fe_3O_4 usando um método hidrotérmico e a estratégia de síntese química com base na 1-etil-3-(3-dimetilaminopropil)carbodiimida (EDC). Seguidamente, os grupos amina foram acetilados usando anidrido acético, obtendo-se os produtos finais (Fe_3O_4/PEI-Ac NGs). Os NGs assim formados mostraram possuir uma boa dispersibilidade e citocompatibilidade. A velocidade de libertação da DOX a partir dos NGs foi estudada, assim como o impacto do pH nesse processo. Os resultados mostraram haver uma libertação sustentada do fármaco que atinge velocidades superiores a valores ácidos de pH. Adicionalmente, estudos realizados *in vitro* com a linha celular tumoral 4T1 mostraram que os Fe_3O_4/PEI-Ac NGs não são citotóxicos, ao contrário do que acontece com os complexos Fe_3O_4/PEI-Ac NGs/DOX e a DOX livre. Os NGs preparados apresentam uma relaxividade r_1 significativamente aumentada (2.29 $mM^{-1}s^{-1}$) comparativamente com as nanopartículas de Fe_3O_4 livres (1.15 $mM^{-1}s^{-1}$), bem como uma excelente eficiência de encapsulamento de DOX (51.4%). Surpreendentemente, os nanogéis apresentam uma capacidade aumentada para imagiologia de ressonância magnética T_1 e uma elevada eficácia terapêutica, quer *in vitro* usando células tumorais, quer num modelo de tumor (xenoenxerto) *in vivo*.

Palavras chave: Polietilenimina; nanogel; nanopartículas de óxido de ferro; doxorubicina; teranóstica.

CONTENTS

LIST OF ACRONYMS

AA – Antibiotic and antimycotic 100x solution

AG - Alginate

AFM – Atomic force microscopy

BIS – N,N′-methylenebisacrylamide

CCK-8 – Cell Counting Kit-8

CT – Computed tomography

DAPI – 4',6-diamidino-2-phenylindole

DSP – Dextrin nanogels

DLS – Dynamic light scattering

DOX – Doxorubicin

DMEM – Dulbecco's modified Eagle medium

EDC – 1-ethyl-3-(3-dimethylaminopropyl)carbodiimide hydrochloride

EPR – Enhanced permeability and retention

^{18}F-FDG – Fludeoxyglucose

FBS – Fetal bovine serum

HPLC – High-performance liquid chromatography

Kpi – Potassium phosphate buffer

Mw – Molecular weight

MWCO – Molecular weight cut-off

MTT – 3-(4,5-dimethyl-2-thiazolyl)-2,5-diphenyl-2-H-tetrazolium bromide

MTX – Methotrexate

MRI – Magnetic resonance imaging

NGs – Nanogels

NHS – N-hydroxysuccinimide;1-hydroxypyrrolidine-2,5-dione

NMR – Nuclear magnetic resonance

NPs – Nanoparticles

PAI – Photoacoustic imaging

PBS – Phosphate buffered saline

PEI – Polyethylenimine

PEA – (poly(ethylene glycol) bis(3-aminopropyl)terminated)

PET – Positron emission computed tomography

PLL – Poly(L-lysine)

PP – Primaquine phosphate

PPI – Polypropyleneimine

pVSVMP – plasmid DNA expressing vesicular stomatitis virus matrix protein

RGD – Arg-Gly-Asp

SPET – Single-Photon emission computed tomography

TEA – Triethylamine

TGA – Thermal Gravimetric Analysis

UV-Vis – Ultraviolet–visible spectroscopy

LIST OF FIGURES

LIST OF TABLES

CHAPTER 1 – INTRODUCTION

CHAPTER 1 – INTRODUCTION

1.1 Nanogels as a nanoplatform for biomedical applications

In recent years, scientists and researchers have been shedding light on nanomaterials as cancer diagnostic agents and drug delivery carriers. Nanomaterials, such as nanotubes[1,2], spherical micelles[3], quantum dots[4,5], nanofibers[6] and nanogels (NGs)[7], may exhibit intriguing biocompatibility, substantial chemical flexibility and long blood circulation time, rendering them with greater advantages in intracellular and extracellular milieu. Among these most studied biomedical materials, NGs have been widely used due to their prominent biocompatibility[8,9], biodegradability[10], stimuli-responsiveness, high drug loading efficiency and easy uptake by tumor cells[11,12].

1.1.1 Nanogels

NGs are three-dimensional (3D) networks of hydrophilic or amphiphilic polymer chains with massive amounts of internal cavities. The linkage between polymeric chains in the NGs could be covalent bonds or physical interactions, such as ionic crosslinking, hydrogen bonding, *van der Waals* interactions and electrostatic interactions, etc. Several preparation methods, such as electrostatic complexation[13,17], inverse emulsion[18], and double emulsion[19], have been explored to produce smart NGs. NGs, possessing flexible chemical architectures, can be designed as smart nanomaterials with sensitivity to pH[20,21], temperature[22] and photo-thermal variations[23]. Also, the networks in the NGs can be used to mimic extracellular matrix environments and encapsulate labile drugs and genes. Due to their similar properties to human tissues and excellent biocompatibility, NGs are perfect platforms for biomedical applications in drug delivery, gene delivery, wound healing and bioimaging[24].

1.1.2 **Polyethylenimine**

Polyethylenimine (PEI), one kind of amine-rich polymer, is widely used in controlled drug delivery, gene therapy, antimicrobial agents and biomedical imaging[25]. PEI can be divided into two types (linear and branched types) and its molecular weight may vary. The amine groups of PEI provide substantial opportunities to load different organic and inorganic materials for biomedical applications. For example, the amine functionalities of PEI can be used to covalently couple with biomolecules. Additionally, pH-sensitive PEI is suitable for controlled drug release. Moreover, polymeric PEI is capable of binding with negatively charged molecules, such as DNA, RNA and proteins for tissue engineering and gene therapy[25]. It has been suggested that the mechanism of antibacterial effect of PEI is related to the electrostatic interactions between positively charged PEI and negatively charged bacterial cell walls[26]. However, the cationic properties of PEI can lead to serious cytotoxicity to living cells, which limits further potential utilization in biomedical areas. As such, methods for reducing its cytotoxic behavior, which do not drastically affect its functionalities, are highly demanding.

Recently, great progress has been made in developing PEI-based NGs with cationic characteristics and low cytotoxicity. Apart from being a main material to synthesize NGs, PEI can also be used to modulate the surface potential of nanoparticles and allow combination with plasmid DNA. The advances in the development of PEI-based NGs will be presented, including synthesis methods and biomedical applications **(Figure 1)**.

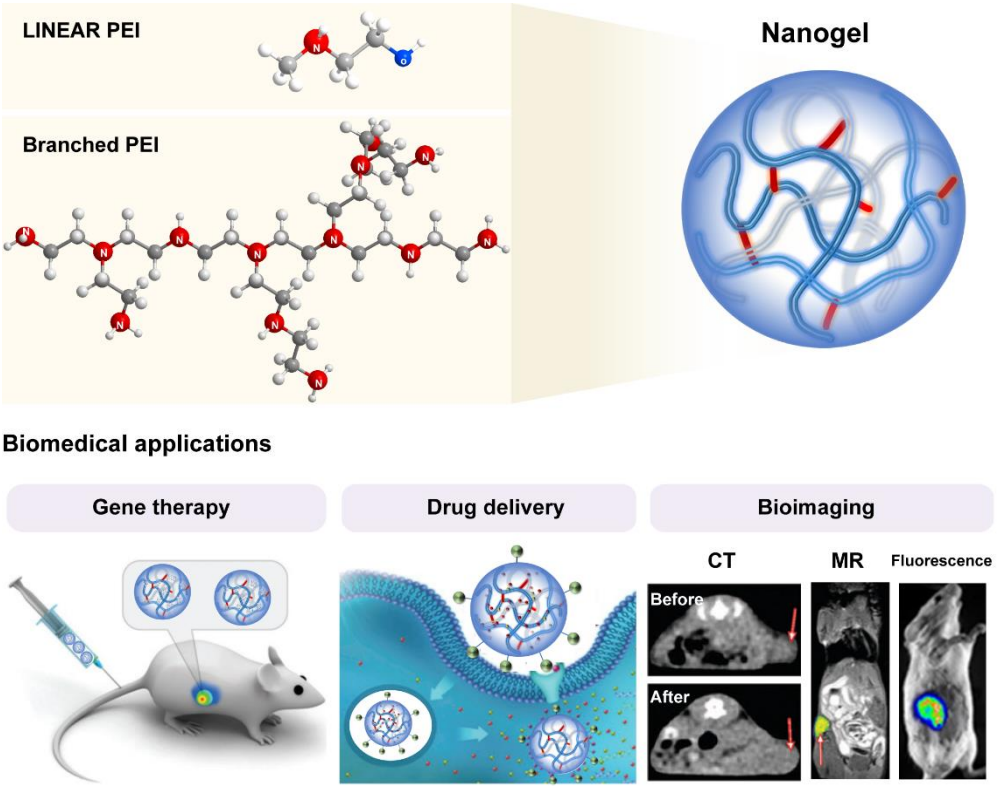

Figure 1. Scheme showing the possible chemical structures of PEI and examples of their biomedical applications in gene delivery, drug delivery and bioimaging. Adapted from ref. [19, 27] Copyright 2018 Elsevier Ltd.

1.2 The synthesis methods of PEI-based NGs

Various methods, such as electrostatic complexation[13-17], inverse-emulsion[18,28,29], self-assembly of biopolymers[10,30] and precipitation polymerization method[20,31,32] can be used to synthesize NGs. With these methods mentioned above, PEI is able to form NGs with large internal cavities and improved dispersion and biocompatibility. Current synthesis methods used for the preparation of PEI-based NGs can be divided into two types: 1) PEI as a base material to form NGs via a) electrostatic interaction and b) crosslinking in a water-in-oil emulsion; 2) PEI as a crosslinker (c) to form NGs composed of other polymer types (**Figure 2**).

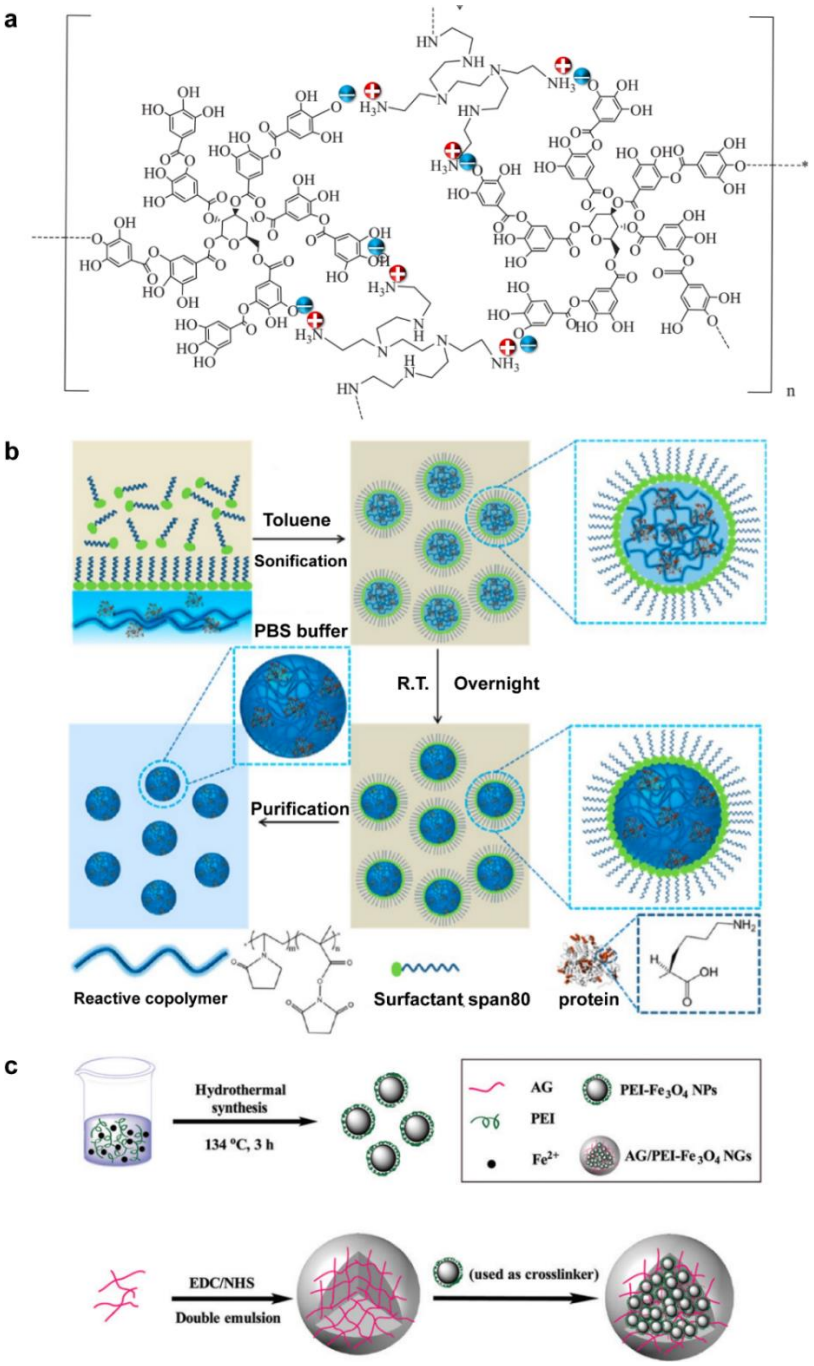

Figure 2. (a) Schematic drawing of tannic acid (TA)/PEI polyplex NGs formed *via* electrostatic interaction. Reproduced with permission[33]. Copyright 2016, Elsevier Ltd. (b) Synthetic procedure to obtain biohybrid NGs *via* crosslinking in W/O emulsion. Reproduced with permission[34]. Copyright 2016, American Chemical Society. (c) Schematic illustration of the formation of PEI-Fe_3O_4 NPs and AG/PEI- Fe_3O_4 NGs. Reproduced with permission[35]. Copyright 2016, The Royal Society of Chemistry.

1.2.1 Electrostatic interaction

The electrostatic self-assembly of NGs involves controlled aggregation of hydrophilic PEI *via* its cationic amine surface with negatively charged polymers. Generally, the preparation is conducted under mild conditions in aqueous environment. Therefore, the electrostatic interactions between PEI and negatively polymers allow encapsulation of various biomolecules inside the NGs. Sahiner *et al.* reported the biodegradable NGs, which have been synthesized by the electrostatic interaction between the phenolic groups of tannic acid (TA) and the positively charged amine groups of PEI[33]. In the preparation of the TA-PEI NGs, they first dissolved PEI in Triton X100/gasoline medium under constant stirring, then mixed with the water solution of TA with the weight ratio of 1:1. The reaction was stopped after 15 min. After precipitation in acetone and being centrifuged at 10000 rpm at room temperature, TA-PEI NGs were obtained. The formed NGs demonstrated highly antioxidant and antimicrobial properties (**Figure 2a**).

1.2.2 Water-in-oil emulsion

Water-in-oil emulsion can also be called as inverse emulsion. The major difference distinguishing water-in-oil emulsion from other emulsion methods is that the water phase is mixed in the oil phase during emulsification. Water-in-oil emulsion provides a new strategy to control the size of the NGs. In this method, PEI determines the chemical properties of the formed NGs, while the reaction conditions decide their physical properties. Peng *et al.* synthesized NGs by crosslinking between poly(N-vinylpyrrolidone) (PVP) and PEI in water-in-oil emulsion. The aqueous phase had PVP and PEI in potassium phosphate (Kpi) buffer and the organic phase consisted of span80 and toluene (**Figure 2b**) to form the NGs in water-in-oil emulsion[34]. In this study, the polymeric NGs crosslinked by PEI showed a spherical morphology and the size of the NGs decreased with an increase of the crosslinking degree.

1.2.3 PEI as a crosslinker

In addition to the physical interaction methods mentioned above, crosslinking of polymer chains provides various opportunities to produce NGs[36]. Sun *et al.* reported the fabrication of magnetic alginate (AG) NGs using PEI-coated iron oxide (Fe_3O_4) nanoparticles (PEI-Fe_3O_4 NPs) as a crosslinker[35]. They found that AG/PEI-Fe_3O_4 NGs were water dispersible, colloidally stable and biocompatible. When compared with PEI-Fe_3O_4 NPs, AG/PEI-Fe_3O_4 NGs showed higher cancer cell uptake ability due to the softness and fluidity of the NGs (Figure 2c). Similarly, Zhu *et al.* utilized γ-polyglutamic acid (γ-PGA) as an alternative and synthesized γ-PGA/PEI-Fe_3O_4 NGs[37]. In these studies, the carboxyl groups of γ-PGA or AG were activated by 1-(3-dimethylaminopropyl)-3-ethylcarbodiimide hydrochloride (EDC), followed by a double emulsion process to generate the γ-PGA or AG NGs. Then, through a dehydration condensation reaction between the carboxyl groups of γ-PGA or AG and the amine groups of PEI-coated Fe_3O_4 NPs, the final NG products were formed.

1.3 Biomedical applications of the PEI-based NGs

1.3.1 Gene therapy

Gene therapy can be defined as the transfer of genetic material into specific cells for disease treatment. It is an effective approach to introduce new genes or replace deficient genes within affected cells. Gene therapies are flourishing around many applications, like cardiovascular and infectious diseases, as well as cancer therapy[38]. For these applications, a high level of the expressed gene is crucial. Gene delivery vehicles can be categorized as recombinant viruses and synthetic vectors. In the process of gene transfection, viruses have attracted wide attention for their high transfection efficiency. However, severe side effects of viruses such as high toxicity and immunogenicity limit their clinical application[39]. Compared

with viral vectors, non-viral vectors are relatively safe, exerting much lower cytotoxicity and immunogenicity, and are easier to be used and produced.

PEI, one of the most effective non-viral gene vectors, has been used over the last two decades. Due to the excellent performance of PEI in gene transfection, researchers have applied PEI-containing NGs in gene delivery[27,38-58]. In general, vectors like PEI-based NGs bind DNA or RNA electrostatically, condensing the genetic materials into particles within hundreds of nanometers, protecting the genes and mediating effective cellular uptake.

For gene transfection, both plasmid and siRNA are frequently used as gene drugs. Qian and coworkers firstly reported heparin-PEI NGs that can be used to transfer the plasmid DNA expressing vesicular stomatitis virus matrix protein (pVSVMP)[38]. These NGs prevent DNA or RNA from being degraded in the transfection process, overcoming a huge problem in gene therapy. The same authors constructed pDNA encoding interleukin-15 (IL15) and used heparin-PEI NGs as a vector to deliver the pDNA for cancer therapy application. After the malignant melanoma (B16) and colon carcinoma (CT26) were treated with heparin-PEI NGs/pDNA polyplexes, the lung metastasis was significantly inhibited with low level of systemic toxicity[59]. In further work, heparin-PEI NGs were used as carriers to deliver the heparan sulfate 6-O-endosulfatase 1 gene that can be used to inhibit tumorgenesis[60,61]. To further enhance gene delivery efficiency, the same group developed a new gene delivery system of PEI-RRRRRRRR(R8)-heparin (HPR) NGs. In their work, heparin and cell penetrating peptide R8 were grafted on PEI with low molecular weight[62]. The formed HPR/pDNA NGs delivered the plasmid DNA encoding human TNF-related apoptosis ligand (phTRAIL) to HCT-116 cells to induce cell apoptosis. In addition, HPR/phTRAIL displayed antitumor capability towards the abdominal metastatic colon carcinoma model, showing a promising future for gene therapy.

PEI (Mw = 25 kDa) has a perfect performance in neutralizing and condensing negatively charged genes, thus protecting them from degradation. However, thick and condensed PEI-

based NGs formed with a large Mw PEI have high cytotoxicity, immunogenicity and slow clearance rate [63,64], and the cargos loaded with gene and drug are more difficult to be released inside tumor cells[65,66]. Considering these situations, Li *et al.* covalently conjugated PEI (with a low Mw of 1.8 kDa) with dextrin via a disulfide bond to form bioreduction-responsive NGs (dextrin NGs, denoted as DSP) for Bcl2 siRNA delivery. Using this system, they achieved a controlled release of Bcl2 siRNA into the cancer cells[27]. They showed that DSP/siRNA labelled with Cy5 displayed the strongest fluorescence intensity after 12 h post injection. Furthermore, DSP/Bcl2 siRNA significantly suppressed Bcl2 protein expression compared with control group (**Figure 3**).

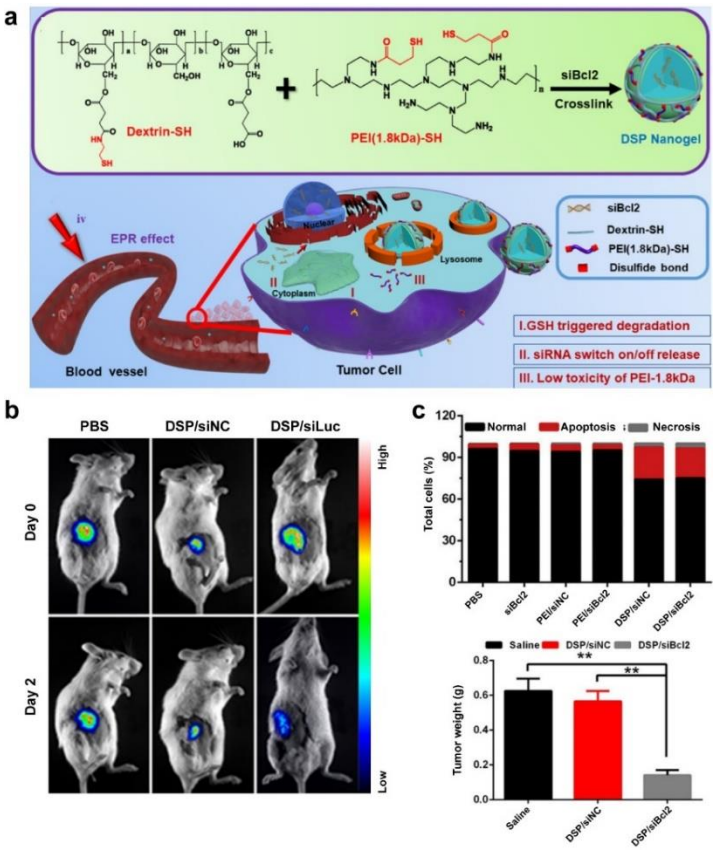

Figure 3. (a) Schematic illustration of reduction-sensitive DSP for siRNA delivery. (b) *In vivo* imaging of DSP/siRNA. (c) *In vitro* apoptosis analysis and *in vivo* tumor suppression study. Reprinted from ref.[27] Copyright 2018 Elsevier B.V.

In a different approach, Costa *et al.* formulated photodegradable PEI-based NGs, allowing for controlled release of different plasmids (pVAX1-*LacZ* and pcDNA3-FLAG-p53) and anticancer drugs such as doxorubicin (DOX), epirubicin (EPIR) and paclitaxel (PTX)[42]. In

their study, they found that ethylene glycol ethers photooxidize in the presence of sunlight, so they used ethylene glycol diglycidyl ether as a crosslinker to confer photodegradable ability to the NGs[42]. PEI NGs condense and stabilize plasmid DNA to form complexes[38,67]. *In vitro* anticancer assay data revealed that the synergistic tumoral treatment through pcDNA3-FLAG-p53 gene and anticancer drug significantly suppressed the viability of cancer cells.

Dimde *et al*. reported a pH-sensitive NG platform for gene delivery using pH-cleavable dendritic polyglycerol-amines (dPG) and low molecular-weight PEI-acrylamide (600 Da) to encapsulate siRNA[40]. These tailor-made NGs were formed through thiol-Michael nanoprecipitation method. The incorporation of pH-sensitive benzacetal-moieties inside the NG network enables the controlled intracellular release of the cargo. *In vitro* GFP-siRNA (green fluorescent protein) transfection assay showed that this network could silence up to 71% GFP expression in HeLa cells.

1.3.2 Drug delivery

NGs are important vehicles in drug delivery due to their reduced clearance rate and longer retention time. Normally, small drug molecules have a short circulation time in the serum and can be cleared from body rapidly. As such, NGs can be excellent drug carriers to increase drug concentration and prolong drug retention time *in vivo*[68]. In addition, NGs can control the drug release rate through their network mesh size and molecular interactions, such as electrostatic and covalent interactions[69]. Through functionalization, they can locally release drugs and reduce off-target treatment and side effects. Moreover, NGs can entrap hydrophobic and hydrophilic drugs and release more than two drugs within one system. NGs display a favorable potency in delivering labile drugs.

Generally, drugs can be incorporated into a NG network by physical encapsulation, covalent conjugation, and controlled self-assembly. On the other hand, drugs can be released from the NGs *via* (a) gradual diffusion, (b) network degradation, (c) variation in pH conditions (or other environmental stimuli, such as temperature, enzyme, etc.), (d) ion displacement, and (e) external energy stimulation (**Figure 4**)[70].

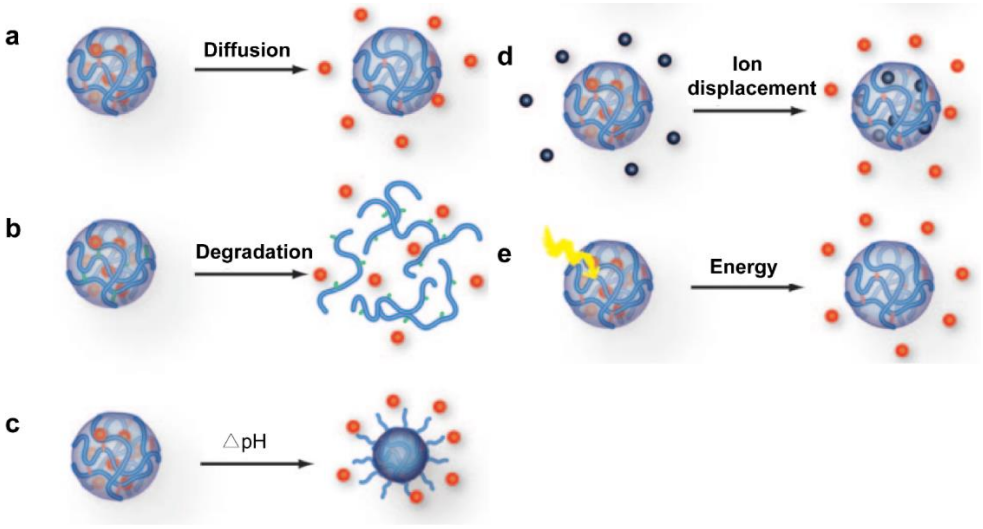

Figure 4. Drug released from NGs in different ways. Reprinted from ref.[70] Copyright 2009 Wiley-VCH Verlag GmbH & Co. KGaA, Weinheim

Vinogradov *et al.* reported cytotoxic nucleoside analog drug delivery, which is based on polyplex NGs (PEI-PEG NGs)[15,69,71,72]. They explored various methods to synthesize PEI-PEG NGs and fabricated an excellent drug and gene delivery system. In this case, PEI-PEG NGs were used to spontaneously encapsulate negatively charged oligonucleotide (ODN), forming a stable aqueous dispersion of polyelectrolyte complexes. They verified that ODN can be effectively transported across the blood-brain barrier (BBB) independently of the specific targeting agent (transferrin or insulin) linked to PEI-PEG NGs. The formed NGs conferred resistance to the ODN against degradation from the immune system.[69] The drug loading efficiency of the synthesized NGs was as high as 33%. This formulation could be a promising drug delivery system, exhibiting an efficient therapeutic activity without systemic toxicity.

In another work, Li *et al.* reported the preparation of Pluronic F127 micelles crosslinked by PEI to form F127/PEI NGs, and incorporated with the hydrophobic anticancer drugs paclitaxel (PTX) and 10-hydroxycamptothecin (HCPT)[73]. The F127/PEI NGs were synthesized by emulsification/solvent evaporation method. The drug and lyophilized empty NGs were dissolved in chloroform. After rotary vacuum evaporation, further lyophilization, hydration with 2-[4-(2-Hydroxyethyl)-1-piperazinyl]ethanesulfonic acid(HEPES)-buffered saline and filtration through nylon filter, the filtrate was lyophilized to get the drug-loaded F127/PEI NGs. The drug-loaded F127/PEI NGs showed a continued *in vitro* drug release profile compared with the free drug. According to the cytotoxicity results, drug-loaded NGs exhibited much higher cytotoxicity against cancer cells *in vitro* than free drugs. The drug-loaded NGs presented greater stability, better cellular uptake and increased solubility[73].

Wu *et al.* used thiolated AG and stearoyl-derivatized PEI to form dual-sensitive (pH-sensitive and redox-sensitive upon exposure to glutathione (GSH)) fluorescent branched AG-PEI copolymer (bAPSC) NGs[74]. bAPSC NGs were synthesized from branched PEI and AG through an amidation reaction using EDC/NHS. The bAPSC NGs were used to load DOX through ultrasonication and aqueous dialysis methods. The bAPSC NGs had a size of around 130 nm and negative surface potential (as shown in **Figure 5a**). Through characterization by UV-vis spectroscopy, the drug loading efficiency and drug loading content of the DOX was calculated to be 11.2% and 25.9%, respectively. The results of release kinetic studies (as shown in **Figure 5b**) showed that the bAPSC NGs were pH-sensitive and GSH-sensitive, and the drug could be rapidly released under acid pH condition in the presence of GSH. Cell viability assays (as shown in **Figure 5c**) showed that the bAPSC NGs/DOX displayed less cytotoxicity than free DOX, possibly due to the sustained release of the DOX from the NGs.

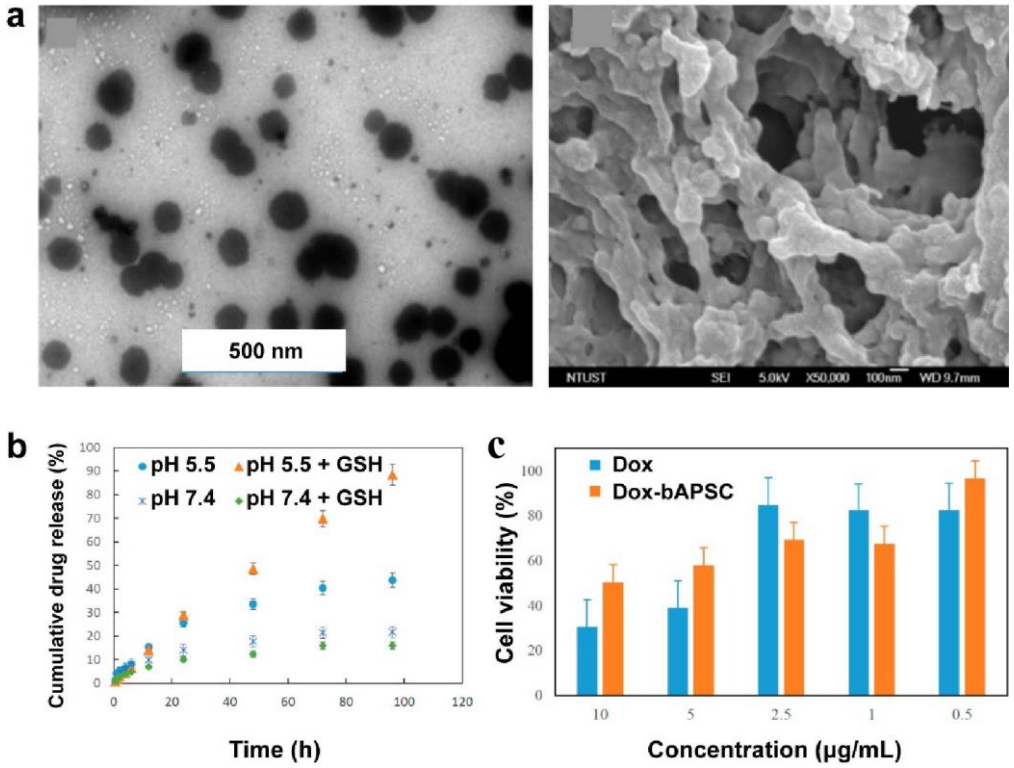

Figure 5. (a) TEM and SEM images of DOX-loaded bAPSC NGs. (b) *In vitro* drug release from DOX-loaded bAPSC NGs (left); *In vitro* toxicity assay of HeLa cells incubated with DOX and DOX-loaded bAPSC NGs (right). Reprinted from ref.[74] Copyright 2017 Multidisciplinary Digital Publishing Institute AG.

1.3.3 Molecular Imaging

Recently, various nanomaterials have been developed for early-stage detection of cancer with different imaging techniques[75,76], such as magnetic resonance (MR)[77-79], computed tomography (CT)[80-82], positron emission computed tomography (PET)[83-85], single-photon emission computed tomography (SPECT)[86-88], photoacoustic imaging (PAI)[89-90]. Each imaging technique has its advantages and cannot be completely replaced by the other technologies. Contrast agents (CAs) are indispensable auxiliary tools for efficient and accurate diagnosis in molecular imaging. For instance, gadolinium-diethylenetriamine pentaacetic acid (Gd-DTPA) can be used for MR imaging[91-92], Omnipaque for CT imaging[93], fludeoxyglucose (^{18}F-FDG) for PET imaging[94-95]. Clinical applications of these contrast agents are limited due to their renal toxicity, lack of targeting specificity and short circulation time. When combined with NGs, CAs

show significant improvements in imaging performance.

CT imaging possesses great advantages in spatial resolution, high density resolution, easy operation and cost effectiveness. In CT imaging, contrast agents are indispensable to improve X-ray attenuation and further locate disease areas. Shi and coworkers synthesized Au NP-loaded γ-PGA NGs by a double emulsion approach[96]. Through the *in-situ* EDC-mediated crosslinking of the amine groups of PEI-entrapped Au NPs and carboxyl groups of γ-PGA, the NGs were formed with a size of 108.6 ± 19.14 nm. The formed γ-PGA−[$(Au_0)_{200}$−PEI·NH_2−mPEG] NGs presented greater X-ray attenuation when compared to commercial iodinated small molecular contrast agents (e.g., Omnipaque). Furthermore, the cellular uptake of the formed NGs was more significant than γ-PGA-stabilized single Au NPs at the same concentration. The formed NGs presented a great potential to be employed as efficient contrast agents for CT imaging of cancer cells *in vitro* and in a xenografted tumor model *in vivo* (**Figure 6**).

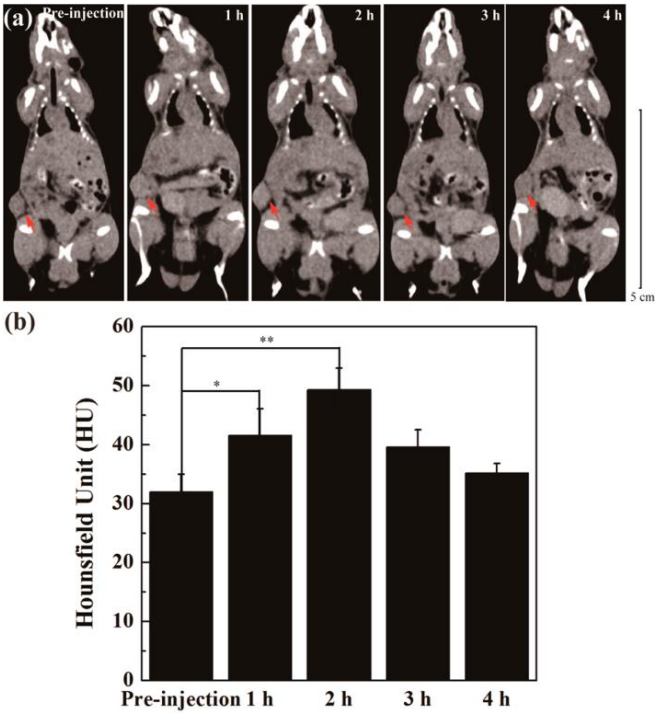

Figure 6. (a) CT images and (b) tumor CT values of the nude mice bearing xenografted HeLa tumor at different time points postintravenous injection of the γ-PGA-[$(Au^0)_{200}$-PEI.NH_2-*m*PEG NGs. Reprinted from ref.[96] Copyright 2017 American Chemical Society.

To promote the use of NGs for other imaging applications, the Shi group reported the preparation of PEI-crosslinked AG NGs incorporated with Fe_3O_4 NPs for MR imaging applications[35]. Firstly, PEI-stabilized Fe_3O_4 NPs were synthesized *via* a hydrothermal method. Then, the carboxyl groups of AG were activated by EDC. After double emulsion to form the AG NGs, PEI-stabilized Fe_3O_4 NPs were used as a crosslinker between the amine group of PEI-Fe_3O_4 NPs and carboxyl groups of AG NGs. The final hybrid NGs presented good water dispersibility, colloidally stability, and were easy uptaken by tumor cells. This kind of hybrid NGs could enhance T_2-weighted MR imaging of cancer cells *in vitro* and in a xenografted tumor model *in vivo*. Similarly, in another work[35], the authors were able to incorporate PEI-stabilized Fe_3O_4 NPs synthesized via a mild reduction method within PGA NGs to have an r_2 relaxivity of 170.87 $mM^{-1}s^{-1}$ for MR imaging of tumors.

For T_1-weighted MR imaging[97,98], Sun *et al.* formed AG-based NGs containing PEI-Mn_3O_4 NPs using the same approach[97]. The size of the formed NGs was about 141.6 nm. The hybrid NGs displayed an r_1 relaxivity (26.12 $mM^{-1}s^{-1}$), which is 19.5 times higher than that of PEI-Mn_3O_4 NPs. Within the nanogels, the incorporated Mn_3O_4 NPs are able to be used for MR imaging in a xenografted tumor model *in vivo* with significantly better sensitivity than the PEI.Ac-Mn_3O_4 NPs.

To further promote the use of NGs for dual mode CT/MR imaging, the Shi group used PEI as a scaffold that was first modified with PEG for entrapment of Au NPs and surface Gd chelation. Then the functionalized PEI was used as crosslinker to prepare hybrid AG/PEI-Au-Gd NGs[19]. The formed AG/PEI-Au-Gd NGs showed a higher r_1 relaxivity (9.16 mM^{-1} s^{-1}) than acetylated PEI-Au-Gd NPs (PEI.Ac-Au-Gd NPs) and the clinical MR contrast agent (Magnevist), and greater X-ray attenuation performance than conventional iodinated CT contrast agents (Omnipaque). Furthermore, the NGs are more prone to be taken up by cancer cells when compared with PEI.Ac-Au-Gd NPs, and enable effective dual mode MR/CT imaging

of cancer cells *in vitro* as well as in a xenografted tumor model *in vivo* (**Figure 7**).

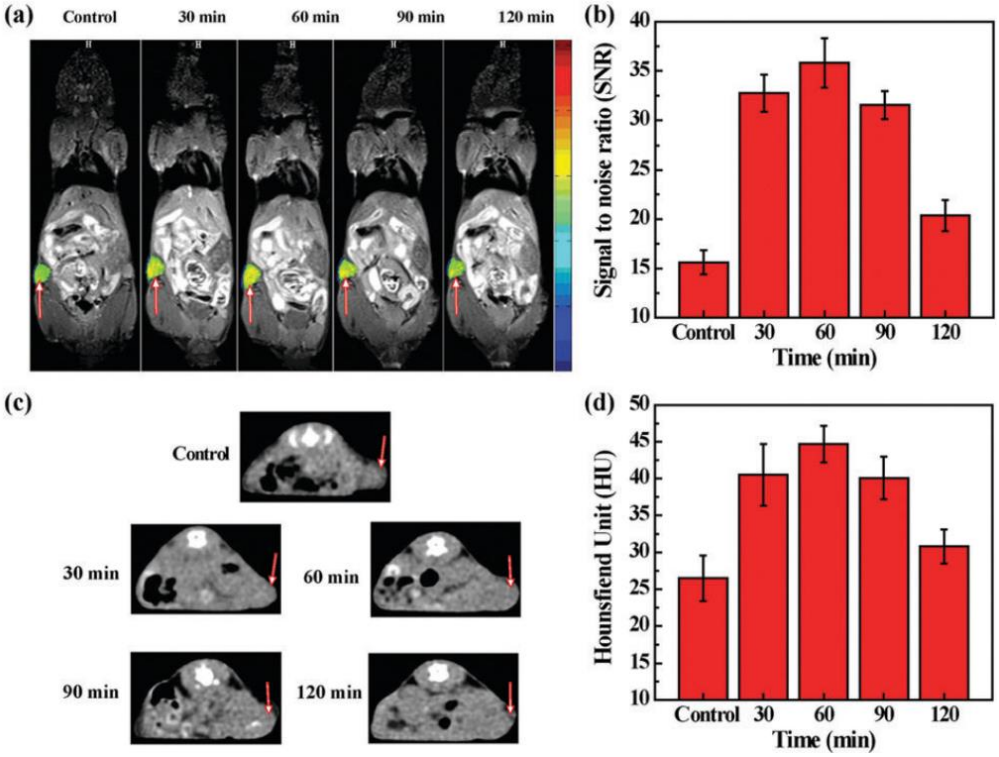

Figure 7. *In vivo* T_1-weighted MR images (a), MR SNR (b), CT images (c), and CT values (d) of xenografted HeLa tumor-bearing mice before and at different time points post intravenous injection of the AG/PEI-Au-Gd NGs. Reprinted from ref.[52] Copyright 2018 The Royal Society of Chemistry.

1.4 Objectives and General strategy of this thesis

The main goal of this study was to synthesize PEI-based NGs loaded with both MR contrast agent ultrasmall Fe_3O_4 NPs and anticancer drug DOX as a tumor theranostic nanoplatform. As shown in **Figure 8**, firstly, ultrasmall Fe_3O_4 NPs were synthesized through a solvothermal method. Secondly, the PEI NGs were prepared *via* a mini-inverse emulsion method and crosslinked by N,N′-methylenebisacrylamide (BIS) via Michael addition. After that, the carboxyl groups of the ultrasmall Fe_3O_4 were activated by EDC/NHS, and then conjugated with the amine groups on the PEI NG surface. Then, the rest of amine groups of NGs were acetylated by triethylamine/acetic anhydride. After physical adsorption of DOX, Fe_3O_4/PEI-Ac

NGs/DOX complexes were obtained. The release kinetics of DOX and the r_1 relaxivity of the NGs were also investigated. After synthesis and the characterization of the final product, *in vitro* and *in vivo* studies were performed to investigate the therapeutic efficacy and imaging capability of the final product. 4T1 tumor cells and BALB/c nude mice were used.

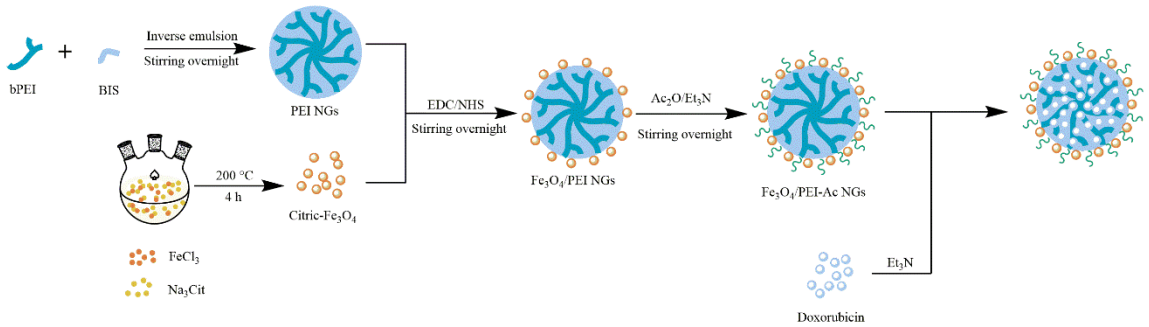

Figure 8 – Synthesis procedure of the Fe_3O_4/PEI-Ac NGs/DOX.

CHAPTER 2 – MATERIALS AND METHODS

CHAPTER 2 – MATERIALS AND METHODS

1.5 Materials and reagents

Branced PEI (bPEI; Mw = 2.5k), BIS and Span® 80 were purchased from SIGMA-ALDRICH (St. Louis, MO). The EDC and NHS were purchased from J&K Scientific Ltd. (Shanghai, China) Triethylamine, acetic anhydride and toluene were purchased from Aladdin Ltd. (Shanghai, China). All other chemicals were obtained from Suzhou Yacoo Science Co., Ltd. (Suzhou, China). Unless otherwise stated, all chemicals were used as received. Cell culture dishes were from Corning Incorporation (New York, NY). 4T1 cells were from Shanghai Institute of Biochemistry and Cell Biology, Chinese Academy of Sciences (Shanghai, China). Dulbecco's modified Eagle medium (DMEM) and antibiotic and antimycotic (AA) 100x solution were purchased from Hangzhou Jinoo Biomedical technology Co. Ltd. (Hangzhou, China). Fetal bovine serum (FBS) and trypsin were purchased from Gibco BRL (Gaithersburg, MD). Water used in all experiments was purified using a MilliQ Plus185 water purification system (Millipore Bedford, MA) and presented a resistivity higher than 18.2 MΩ.

1.6 Synthesis of Fe_3O_4/PEI-Ac NGs

Synthesis of citrate-stabilized Fe_3O_4 NPs. Ferric chloride anhydrous ($FeCl_3$, 324.4 mg) was dissolved in 20 mL of diethylene glycol. After ferric chloride was completely dissolved, sodium citrate (235.5 mg) was added under stirring. After the sodium citrate was completely dissolved, the solution was put into a water bath at 80 ℃ for 120 min. At the end of the reaction, the solution was cooled down to 55 ℃, and sodium acetate (656 mg) was then added to the mixture solution under stirring to form a transparent solution, which was transferred to the high temperature and high-pressure reactor. The reaction in the reactor was conducted in an oven at 200 ℃ for 4 h. After the reaction was completed, the product was

cooled down to room temperature, centrifuged and purified by washing and redispersed with ethanol. Ultrasmall Fe_3O_4 NPs were formed by lyophilization of the purified product.

Synthesis of PEI NGs. Span® 80 (1.2 g) was dissolved in toluene (60 mL) under stirring at room temperature for 30 min. bPEI (272 mg) and BIS (32 mg) were dissolved in 5 mL of water, dropwise added in the above solution under stirring for 120 min. Ultrasonication was used to achieve emulsification. After that, triethylamine (TEA) as a catalyst was added into solution to initiate PEI crosslinking. The mixture solution was stirred overnight. At the end of the reaction, the NGs were collected by centrifugation (13 000 rpm, 15 min) and redispersion in methanol for 3 times to remove toluene. After that, the product was purified by dialysis against water using a dialysis membrane with a molecular weight cut-off (MWCO) of 8000-14000 for 3 days.

Synthesis of Fe_3O_4/PEI NGs. The ultrasmall Fe_3O_4 NPs (50 mg) synthesized were dispersed in water (5 mL) and their surface carboxyl groups were activated by EDC/NHS (EDC mass = 75 mg, NHS mass = 45 mg). The mixture solution was dropwise added into the solution of PEI NGs (250 mg, 25 mL) under stirring overnight. The product was collected through centrifugation (13000 rpm, 15 min) and redispersed in water for 3 times. Then the product was purified by dialysis against water using a dialysis membrane (MWCO = 8000-14000) for 3 days. After that, the Fe_3O_4/PEI NGs were obtained, which were stored in water at 4 ℃.

Synthesis of Fe_3O_4/PEI-Ac NGs. The Fe_3O_4/PEI NGs were acetylated by acetic anhydride. The triethylamine（134.1 μL）as a catalyst was dropwise added into the solution of the Fe_3O_4/PEI NGs (20 mg, 2 mL) under stirring for 30 min. Then acetic anhydride (75.9 μL) was added into the mixture solution under stirring overnight. The product was purified by membrane dialysis (MWCO = 8000-14000) against water for 2 days, and then were stored at 4 ℃.

Drug loading within Fe_3O_4/PEI-Ac NGs. The Fe_3O_4/PEI-Ac NGs were centrifuged (13000 rpm) and redispersed in PBS (pH = 7.4). Doxorubicin hydrochloride was dissolved in water, and then dropwise added into the solution of Fe_3O_4/PEI-Ac NGs. The mixture solution was stirred overnight in the dark. The final product was collected by centrifugation (13000 rpm) and stored in the dark at 4 ℃.

1.7 Characterization of the Fe_3O_4/PEI-Ac NGs

Thermal gravimetric analysis (TGA): Ultrasmall Fe_3O_4 NPs, Fe_3O_4/PEI NGs and Fe_3O_4/PEI-Ac NGs was analyzed using a TG209F1 Thermal Gravimetric Analyzer (NETZSCH, Selb, Germany). All samples (5ml) were lyophilized to powder before measurements. The samples were then heated from room temperature to 900℃ at the rate of 20℃/min under nitrogen protection.

Hydrodynamic size and zeta-potential: The starting materials and the products from each step were measured using a Nano-ZS (Malvern, Malvern, UK). All the materials and products were dissolved in water. The concentration of the solutions was approximately 10mg/mL.

UV-vis spectra: The spectra were recorded using a Perkin-Elmer Lambda 25 UV-vis spectrophotometer (Boston, MA). All the materials and products were dissolved in water. The concentration used in the UV-vis spectra analysis was dependent on the specific situation.

Atomic force microscope (AFM): The AFM (MFP-3D, Asylum Research, Santa Barbara, CA) was used to characterize the morphology of the materials. The tips used in the measurements were made of SiN. The AFM samples were prepared by dropping diluted sample suspensions, which were diluted 10^6 times from 1mg/mL, on silicon wafers and nitrogen-dried before measurements.

Inductively Coupled Plasma Optical Emission Spectrometer: Leeman Prodigy inductively coupled plasma-optical emission spectroscopy (ICP-OES) was performed to analyze the Fe composition in the NGs (Hudson, NH). All samples were digested by aqua regia and diluted with water before measurements.

Relaxivity: The r_1 relaxivities of the ultrasmall Fe_3O_4 NPs, Fe_3O_4/PEI NGs and Fe_3O_4/PEI-Ac NGs were measured using the 0.5T NMI20-Analyst NMR Analyzing and Imaging system (Shanghai Niumag Corporation, Shanghai, China). The parameters were set as follow: Q-IR sequence, point resolution = 156 mm × 156 mm, section thickness = 0.6 mm, TR = 6000 ms, TE =160 ms, number of excitation = 1. The r_1 relaxivity of the materials were calculated by a linear fitting of the inverse relaxation time as a function of the Fe concentration. The MR imaging of samples was performed using a 3.0T signa HDxt (GE CO., LTD. Milwaukee, WI).

1.8 Encapsulation of DOX within Fe_3O_4/PEI-Ac NGs

The Fe_3O_4/PEI-Ac NGs (10 mg) were dispersed in 1 mL of PBS. DOX at a mass ratio of 0.5, 1 and 2 to Fe_3O_4/PEI-Ac NGs was dissolved in 1 mL water, respectively. Then the Fe_3O_4/PEI-Ac NG solutions were mixed with the DOX solutions under stirring overnight. After that, the mixture solutions were centrifuged (13000 rpm for 15 min) in order to get the precipitates, washed with water for 3 times and the supernatants in each step (containing the non-complexed free DOX) were collected. The precipitates were redispersed in 2 mL of PBS and stored at 4 ℃. The supernatants were analyzed via UV-vis spectroscopy and the encapsulated amount of DOX in the NGs was calculated *via* subtraction of the initial added DOX amount with that in the supernatants.

According to the standard curve of DOX in water, the drug loading content (DLC) and

drug loading efficiency (DLE) were calculated using the following equations, respectively:

$$\mathrm{DLC} = \frac{m_{loading\ drug}}{m_{nanogels}+m_{drug}} \times 100\% \quad (1)$$

$$\mathrm{DLE} = \frac{m_{loading\ drug}}{m_{nanogels}} \times 100\% \quad (2)$$

$m_{loading\ drug}$: the mass of the drug which was loaded in the NGs

m_{drug}: the mass of the drug which was used in the reaction

$m_{nanogel}$: the mass of the NGs which were used in the reaction.

1.9 In vitro drug release kinetic studies

The formed Fe_3O_4/PEI-Ac NGs /DOX solution was diluted to have a DOX concentration of 1 mg/mL in phosphate buffer with different pH values. The dialysis bags with a MWCO of 8 000 – 14 000 were used to hold 1 mL of the diluted Fe_3O_4/PEI-Ac NGs /DOX solution. After well-sealed, the bags were immersed in 9 mL of pH = 7.4 and pH = 5.5 phosphate buffer, respectively. All the systems were placed in a shaker at a constant temperature of 37 °C. At different time points, 1 mL of the outside medium was taken and the absorbance at 480 nm was measured using a UV-vis spectrophotometer. After that, the outer phase was replenished with 1 mL fresh corresponding buffer solution. Finally, the curve of DOX release from the Fe_3O_4/PEI-Ac NGs/DOX under different pH conditions *in vitro* was obtained.

1.10 Cell biological evaluation

In the *in vitro* testing, 4T1 tumor cells (a mammary carcinoma cell line from the mammary gland tissue of a mouse) were continuously grown in the cell culture flask with DMEM supplemented with 10% FBS, 100 U mL^{-1} penicillin, and 100 U mL^{-1} streptomycin. The culture was maintained at 37 °C in a wet incubator with 5 % CO_2, and the medium was replaced every 3 days.

To check if the Fe_3O_4/PEI-Ac NGs /DOX complex was therapeutically active, two days before exposure to the NGs, the cells at logarithmic growth stage were plated into 96-well plates at a density of 1×10^4 cells per well in supplemented DMEM. For the cytotoxicity experiments, the medium was then replaced with fresh DMEM (100 μL) containing free DOX·HCl, Fe_3O_4/PEI-Ac NGs or Fe_3O_4/PEI-Ac NGs /DOX complex with different DOX concentrations (2.5, 5, 10, 20, and 40 μg/mL, respectively). For the DOX-free Fe_3O_4/PEI-Ac NGs, the NG concentration is equal to the Fe_3O_4/PEI-Ac NGs/DOX complex. In all cases, the samples were dissolved in PBS prior to testing. Then the cells were incubated for 24 h at 37 °C. After treatment with DOX or Fe_3O_4/PEI-Ac NGs /DOX complex, cell morphology was observed by optical microscopy. After morphology observation, cell counting kit - 8 (CCK-8) assay was performed to quantify the viability of the cells. Furthermore, PBS was used as a control to check the therapeutic activity of the drug.

To check the cellular uptake of the Fe_3O_4/PEI-Ac NGs /DOX complex, two days before exposure to NGs, the cells at logarithmic growth stage were plated into a glass bottom dish at a density of 15×10^4 cells per dish in supplemented DMEM. The next day, the medium was replaced with supplemented DMEM (200 μL) containing free DOX·HCl or Fe_3O_4/PEI-Ac NGs /DOX complex at the same DOX concentration (10 μg/mL) and then the cells were incubated for 4 h at 37 °C. Only PBS was used in the control. After that, the medium was

dumped, the bottom of the dish was covered with glutaraldehyde (1%, v/v) for 15 min, washed and added of 4′,6-diamidino-2-phenylindole (DAPI, 0.1%, v/v) for cell nucleus staining. After 30 min, the bottom of the dish was washed with PBS to remove DAPI.

Furthermore, to quantify the uptake of the Fe_3O_4/PEI-Ac NGs /DOX complex by cells, two days before exposure to NGs, the cells at logarithmic growth stage were plated into 12-well plates at a density of 15×10^4 cells per well in supplemented DMEM. The next day, the medium was replaced with supplemented DMEM (100 μL) containing free DOX or Fe_3O_4/PEI-Ac NGs /DOX with different DOX concentrations (1.25, 2.5, 5, 10, 20, and 40 μM) and then the cells were incubated for 4 h at 37 °C. After that, the medium was dumped and the cells were washed with PBS for 3 times, collected by centrifugation (1000 rpm, 5min) and resuspended in 1 mL of PBS. All the parallel groups of cells were collected and redispersed for flow cytometry analysis using a BD FACS Calibur flow cytometer (Franklin, CA).

1.11 In vivo tumor therapy and MR imaging

All animal experiments were carried out after approval by the ethical committee for animal care of Donghua University and according to the policy of the National Ministry of Health (China). The female BALB/c nude mice with 4-6 weeks age were purchased from Shanghai Slac Laboratory Animal Center (Shanghai, China). After feeding for one week in a sterile animal room, 4T1 cells were injected into the right hind leg of the nude mice at a dose of 1.5×10^6 cells/mouse. When the tumor volume reached 0.5-1.2 cm^3 (about two weeks after injection of tumor cells), the tumor-bearing nude mice were randomly divided into 4 groups (control group, free DOX group, Fe_3O_4/PEI-Ac NGs /DOX treatment group and non-drug-loaded Fe_3O_4/PEI-Ac NGs group), and each group had 5 mice. On the first day, the

control group, the free DOX group, the treatment group, and the non-drug-loaded group were intravenously injected with PBS (200 μL), free DOX (200 μL in PBS, [DOX] = 20 μg/mL), Fe_3O_4/PEI-Ac NGs/DOX complex (200 μL in PBS, [DOX] = 20 μg/mL), and Fe_3O_4/PEI-Ac NGs (NGs concentration is the same as the treatment group) for each mouse. That day was recorded as the first dose. The materials were administered once every 3 days for a total of 5 doses. Tumor volume was measured every 3 days and mouse weight was weighed every 3 days. Tumor volume and relative tumor volume were calculated using the following equations, respectively:

$$V_{tumor\ volume} = \frac{a \times b^2}{2} \quad (3)$$

where a and b represent the maximum and minimum diameters of the tumor, respectively.

$$\text{Relative tumor volume} = \frac{V}{V_0} \quad (4)$$

where V and V_0 represent the tumor volume after administration and the tumor volume before administration, respectively. Thirty days after the first time of the treatment, representative mice were selected and sacrificed from each group, and their main organs and tumors were extracted.

The Fe distribution in various organs of nude mice at different time points post injection of Fe_3O_4/PEI-Ac NGs/DOX was determined. The PBS buffer solution of Fe_3O_4/PEI-Ac NGs/DOX was injected into the nude mice through intravenous injection (Fe mass = 150 μg, in 200 μL PBS for each mouse), and the mice were sacrificed at different time points post-injection (0.5, 1, 12, 24 and 48 h, respectively). The organs (heart, liver, spleen, lung, kidney) and tumor was removed, weighed, then digested by aqua regia for 24 h. The concentration of Fe in the organ and tumor was measured by ICP-OES. Nude mice injected with only 0.2 mL of PBS solution without Fe_3O_4/PEI-Ac NGs/DOX were used as control. The results of three parallel nude mice were used for each group. Parallel organ or tumor samples were processed according to standard protocols for H&E staining and TUNEL staining after 30

days' treatment.

The BALB/c nude mice were chosen to construct subcutaneous 4T1 tumor model. Each tumor mouse was intravenously injected with a PBS solution containing ultrasmall Fe_3O_4 NPs or Fe_3O_4/PEI-Ac NGs /DOX (Fe mass = 150 μg, in 200 μL PBS). MR scanning was performed using a 3.0T signa HDxt (GE CO., LTD. Milwaukee, WI). to evaluate the tumor imaging performance of the materials. MR scanning parameters were set as follows: wrist ECHO sequence (TR = 376 ms, TE = 10 ms, point resolution = 256 mm × 256 mm, section thickness =5 mm, and FOV = 100 × 100 mm).

1.12 Statistical analysis

One-way ANOVA statistical analysis was performed to evaluate the significance of the experimental data. A value of 0.05 was selected as the significance level, and the data were indicated with (*) for $p < 0.05$, (**) for $p < 0.01$, and (***) for $p < 0.001$, respectively.

CHAPTER 3 – RESULTS AND DISCUSSION

2.1 Characterization of Fe_3O_4/PEI-Ac NGs

TGA analysis. After the citrate-Fe_3O_4 NPs were conjugated with the PEI NGs, TGA was performed to confirm their composition (**Figure 9**). It is clear to see that the weight of citrate-Fe_3O_4 NPs and Fe_3O_4/PEI NGs decreases with the increase of the temperature, and the decrease trend of Fe_3O_4/PEI NGs curve is faster than citrate-Fe_3O_4. During the temperature increase from room temperature to 900 ℃, after simple mathematical calculation, the percentage of citrate-Fe_3O_4 NPs loaded within the PEI-based NGs was estimated to be 55.38% (w/w).

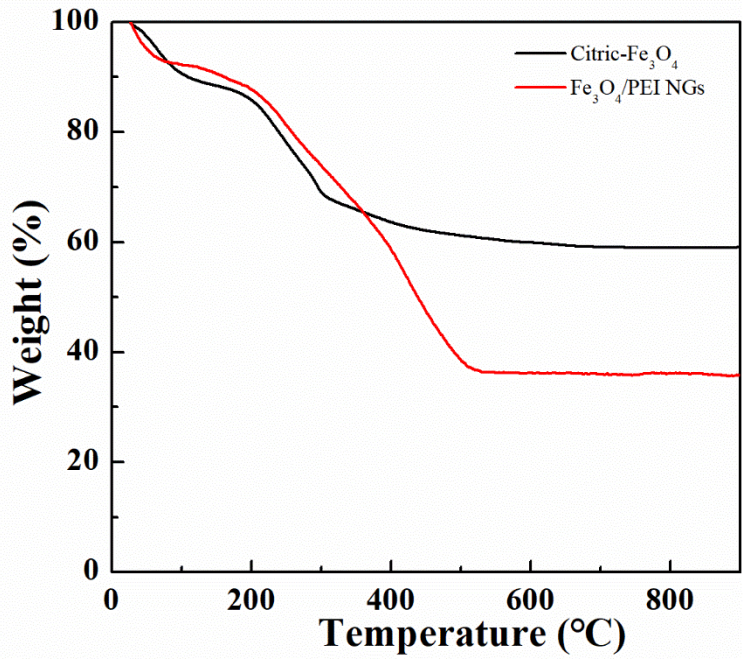

Figure 9. TGA curve of citrate-Fe_3O_4 and Fe_3O_4/PEI NGs.

DLS and zeta potential measurements. To decrease the amine-related cytotoxicity of the NGs, acetylation of the Fe_3O_4/PEI NGs was performed. Through the DLS and zeta-potential analysis of each material involved in the synthesis procedure, the hydrodynamic size and surface potential presented noticeable change. As shown in Table 1, the citrate-Fe_3O_4 NPs

present a negative charge before conjugation, and the PEI NGs are positively charged. After conjugation, the surface potential of the NGs decreases to 29.3 mV. Further acetylation of the NGs leads to a further decrease of the surface potential of the NGs to 13.3 mV. The increasing of the hydrodynamic size after each step of modification confirms the success of each synthesis procedure.

Table 1. Hydrodynamic size and zeta potential of PEI NG, Fe_3O_4/PEI NGs and Fe_3O_4/PEI-Ac NGs.

Sample	Size (nm)	PDI	Zeta Potential (mV)
Fe_3O_4	27.5 ± 3.2	0.162 ± 0.058	-37.9 ± 1.35
PEI NGs	180.38 ± 5.48	0.234 ± 0.024	38.9 ± 0.624
Fe_3O_4/PEI NGs	251.4 ± 6.34	0.242 ± 0.003	29.3 ± 0.88
Fe_3O_4/PEI-Ac NGs	263.8 ± 3.81	0.334 ± 0.03	13.3 ± 1.15

Morphology characterization. AFM was used to observe the morphology of the synthesized NGs. As shown in Figure 10, the size of the PEI-based NGs is around 137 nm, and after conjugation and surface acetylation (Fe_3O_4/PEI-Ac NGs) the size increased to 157 nm while maintaining the same good monodispersity. Apparently, the size of the NGs measured by AFM is different from that measured by DLS. This is because, in the DLS analysis, we got the hydrodynamic size of the materials in a swollen state, while in AFM we measured the size of the NGs in the dried state and the NGs shrinks. It's worth noting that, different from other quasi-spherical nanomaterials, the AFM image of the NGs shows a large flat image, and the height was significantly different from their width, which may be caused by the huge cavity and soft backbone of the NGs.

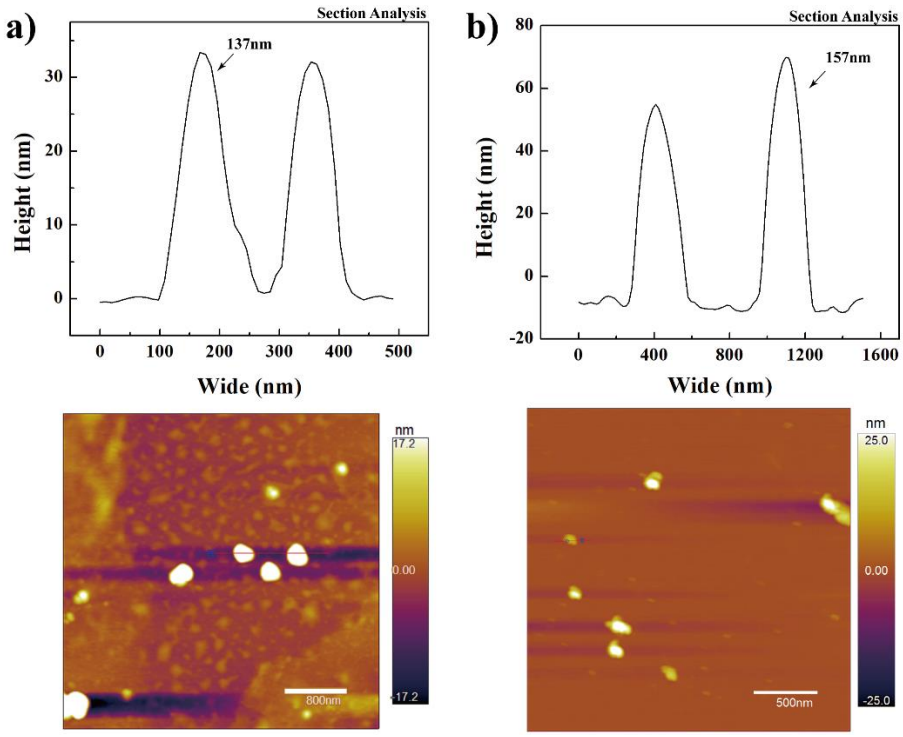

Figure 10. AFM images of a) PEI NGs and b) Fe_3O_4/PEI-Ac NGs.

r_1 relaxivity characterization. Because the size of citrate-stabilized Fe_3O_4 NPs, which were synthesized by Solvothermal method, is lower than 5 nm, the formed ultrasmall Fe_3O_4 NPs are well suitable for T_1-weighted MR imaging[99]. MR phantom studies show that both materials enable MR contrast enhancement in an Fe concentration-dependent manner. The Fe_3O_4/PEI-Ac NGs seem to display a higher MR signal intensity than the citrate-stabilized Fe_3O_4 NPs under the same Fe concentrations. We then measured the r_1 relaxivities of the citrate-stabilized Fe_3O_4 NPs and Fe_3O_4/PEI-Ac NGs. As shown in Figure 11b, the r_1 relaxivity of citrate-Fe_3O_4 NPs was measured to be 1.15 $mM^{-1}s^{-1}$. After the conjugation onto PEI-based NGs, the formed hybrid NGs show a higher r_1 relaxivity (2.29 $mM^{-1}s^{-1}$) than the citrate-stabilized Fe_3O_4 NPs. This is due to the fact that the citrate-stabilized Fe_3O_4 NPs, once entrapped within the NGs, could have a relatively longer rotational correlation time, thus presenting an increased r_1 relaxivity, which is beneficial for improved MR imaging sensitivity.

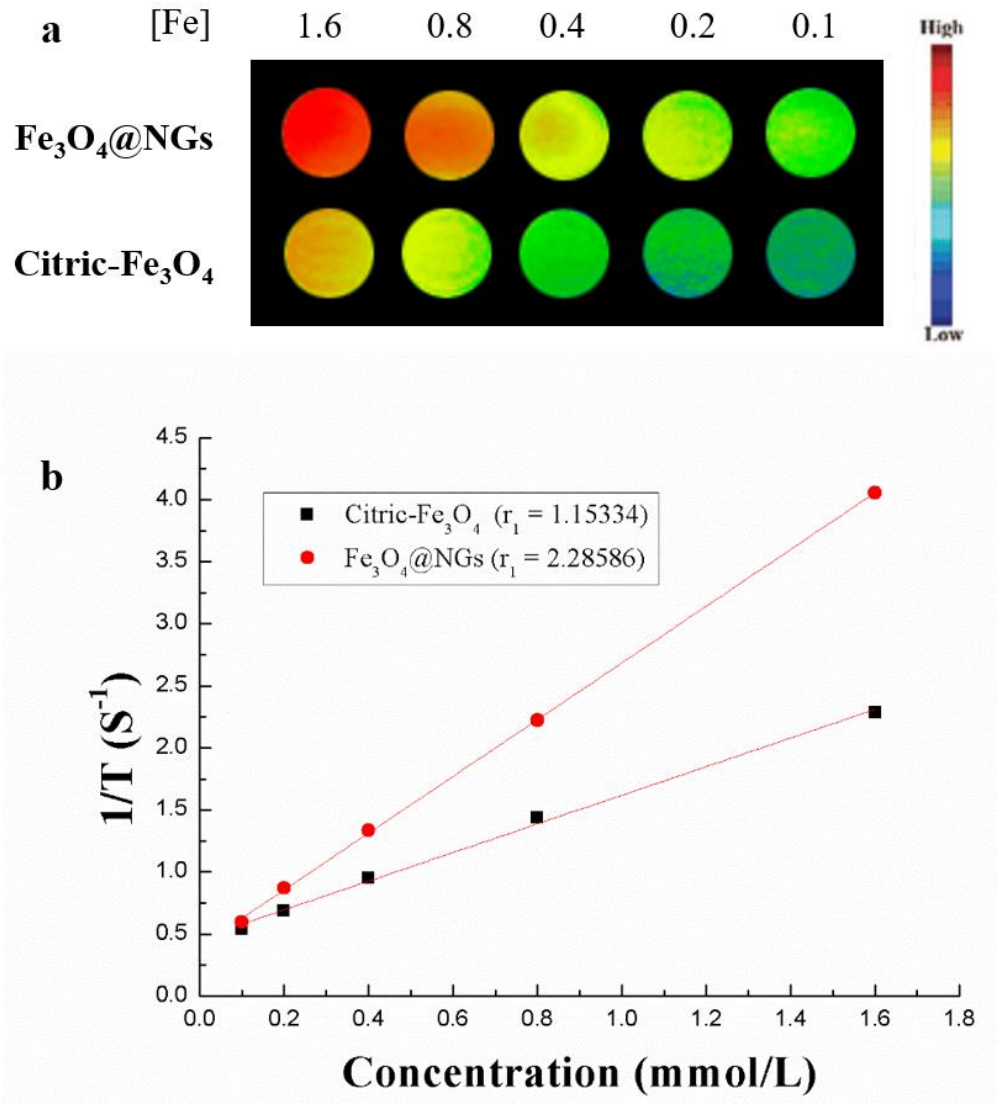

Figure 11. a) Color T_1-weighted MR images of the citrate-Fe_3O_4 NPs and Fe_3O_4/PEI-Ac NGs at an Fe concentration of 0.1, 0.2, 0.4, 0.8, and 1.6 mM, respectively. b) Linear fitting of $1/T_1$ as a function of Fe concentration for the two different materials. The color bar from red to blue indicates the gradual decrease of MR signal intensity.

2.2 Encapsulation of DOX within the Fe_3O_4/PEI-Ac NGs

The DOX loading efficiency and loading content within the Fe_3O_4/PEI-Ac NGs were obtained by measurement of the non-complexed free DOX in supernatant that was recovered by centrifugation via UV-Vis spectroscopy. First of all, we got the standard curve of DOX absorption at 478 nm versus DOX concentration in PBS solution (Figure 12).

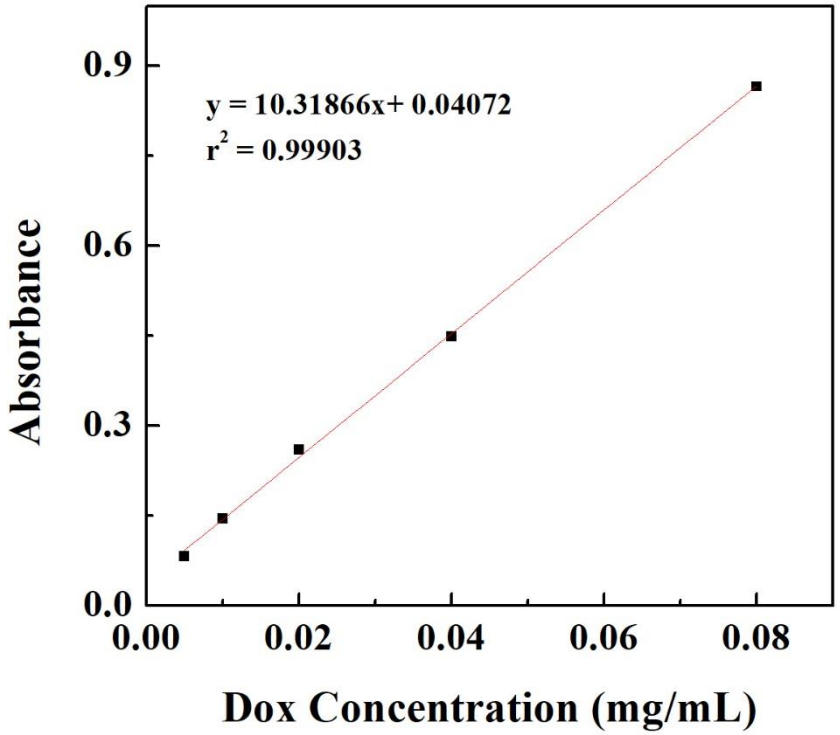

Figure 12. Standard absorption-concentration calibration curve of DOX in PBS (pH = 7.4).

Secondly, we optimized ratios between DOX and Fe_3O_4/PEI-Ac NGs during the drug loading process. The Fe_3O_4/PEI-Ac NGs/DOX formed at different mass ratios between DOX and the NGs (1:2, 1:1, or 2:1) were measured by UV-vis spectrometry based on the standard calibration curve. As shown in Table 2, the mass ratio of DOX:NGs at 1:1 presents the best loading content when compared with others, while the mass ratio of 2:1 presents the greatest loading efficiency. According to the results, we selected the ratio of 2:1 as the optimized ratio for the subsequent experiment.

Table 2. The DLC and the DLE of Fe_3O_4/PEI-Ac NGs/DOX.

Mass ratio (DOX: NGs)	DLC	DLE
1:2	15.3%	22.9%
1:1	21.9%	43.9%
2:1	18.3%	51.4%

2.3 In vitro release kinetic studies

The *in vitro* release study of DOX from the Fe_3O_4/PEI-Ac NGs/DOX complexes was performed in phosphate buffer with different pH values (5.5 and 7.4) and the temperature was kept at 37℃. In each case, the release of DOX from the complexes showed a sustained release profile. The cumulative release of DOX from the Fe_3O_4/PEI-Ac NGs/DOX in a weakly acidic environment of pH = 5.5 was 44.1 ± 2.05%, which was higher than that in a physiological environment with pH = 7.4. This result indicates that the PEI-based NGs have pH-responsiveness, and DOX can be rapidly released in the slightly acidic environment which is similar to tumor tissue, and slow release rate and low cumulative release rate in the physiological environment of normal tissues. This is certainly beneficial for desired tumor treatment.

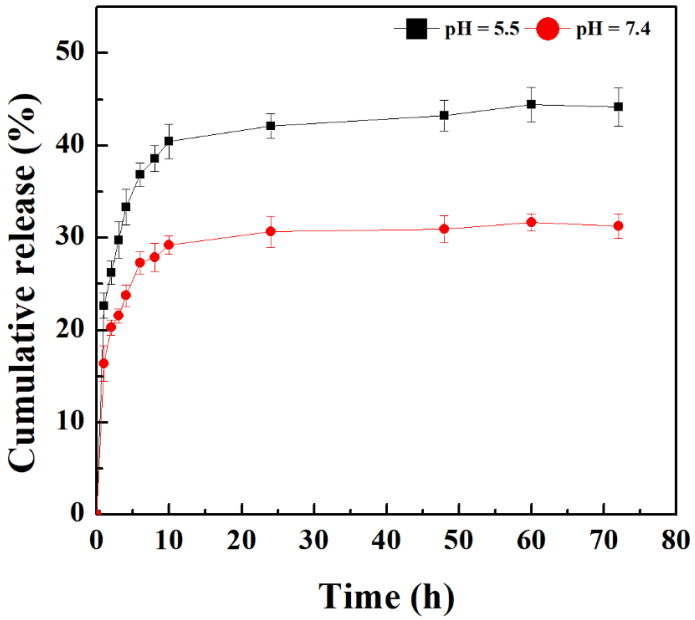

Figure 13. Cumulative release of DOX from Fe_3O_4/PEI-Ac NGs/DOX complexes under different pHs.

2.4 Therapeutic efficacy of DOX encapsulated within Fe_3O_4/PEI-Ac NGs

The therapeutic efficacy of the DOX encapsulated within the Fe_3O_4/PEI-Ac NGs on 4T1 tumor cells was tested using the CCK-8 assay (**Figure 14**). It is clear that the cell viability of free DOX group is much lower than that of the Fe_3O_4/PEI-Ac NGs/DOX group, which is due to the slow release of the DOX from the NGs. In both cases, the cell viability decreases with the increase of DOX concentration. For the drug-free Fe_3O_4/PEI-Ac NGs, under the studied NG concentrations, the cell viability does not seem to have a significant change when compared to the PBS control. So, the Fe_3O_4/PEI-Ac NGs show good cytocompatibility.

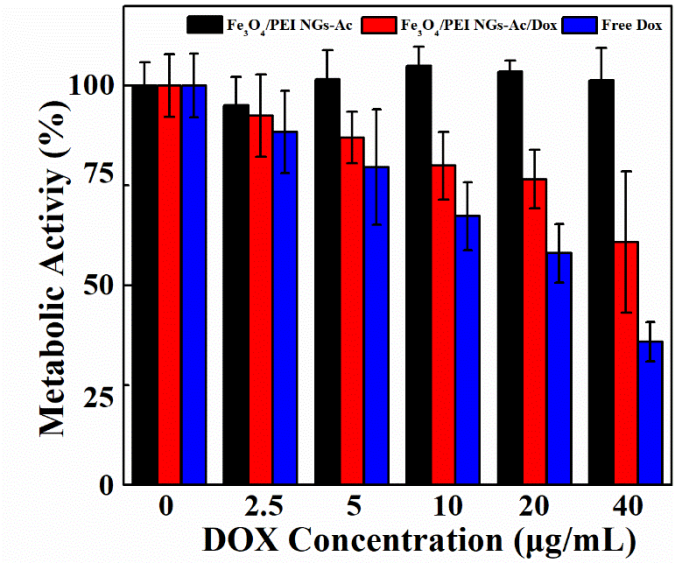

Figure 14. CCK-8 assay of 4T1 cell viability after they were treated with Fe_3O_4/PEI-Ac NGs/DOX, free DOX and Fe_3O_4/PEI-Ac NGs at different DOX or NG concentrations for 24 h. The 4T1 cells treated with PBS were used as a control.

2.5 Cellular uptake of the Fe_3O_4/PEI-Ac NGs/DOX complex

To check the cellular uptake of DOX-loaded NGs, confocal laser scanning microscopy and flow cytometry were performed. After DAPI staining, PBS group just shows the blue fluorescence of the nuclei stained by DAPI (As shown in **Figure 15**). The free DOX group shows the blue fluorescence from DAPI and the red fluorescence from DOX. After merging those two, the cells from free DOX group showed purple nuclei and red cytoplasm, the purple of the nuclei is caused by the mixture of red and blue. This implies that free DOX is

able to enter to the cell nuclei. For the group of Fe_3O_4/PEI-Ac NGs/DOX, obvious blue and red fluorescence can also be seen, but the majority of DOX-associated red fluorescence appears in the cytoplasm, not in the cell nuclei. This implies that DOX was released from the NGs before getting into the cell nuclei, which takes time.

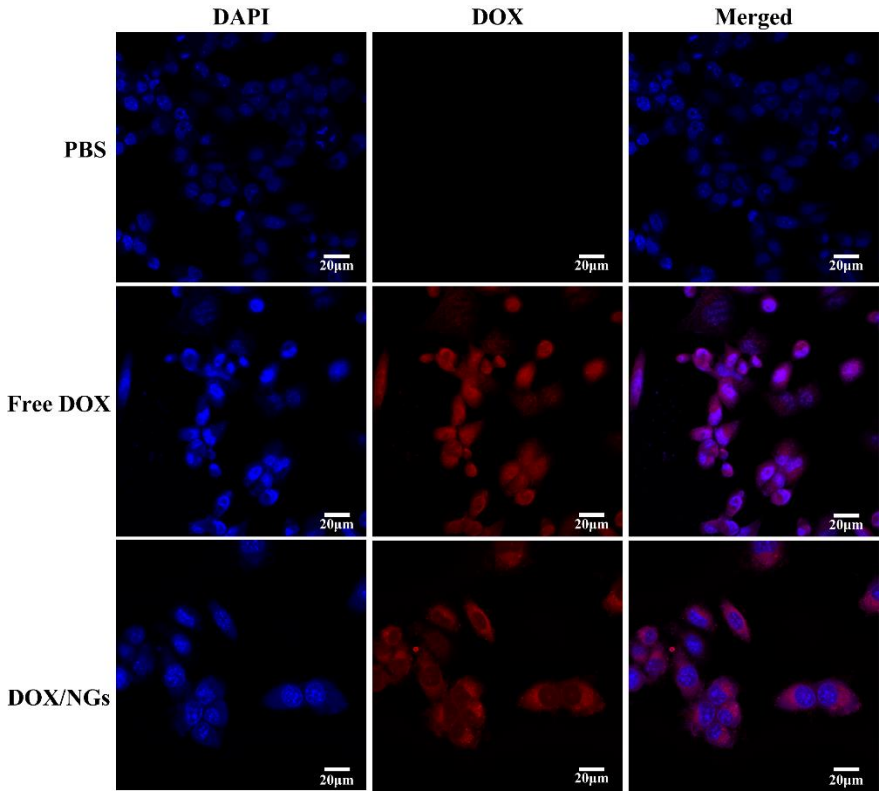

Figure 15. Confocal microscopic images of 4T1 cells after treatment for 4 h with the free DOX and Fe_3O_4/PEI-Ac NGs/DOX at a DOX concentration of 10 μg/mL. The 4T1 cells treated with PBS were used as a control.

Flow cytometry analysis was further used to confirm the cellular uptake of the DOX-loaded NGs (**Figure 16**). The right shifted histogram shown in the left panel of Figure 16 indicate that the cells are able to take up the NGs to display DOX-associated fluorescence signal. With the increase of DOX concentration, the cell fluorescence histogram displays more apparent right shift trend, indicating that there are more NGs uptaken by cells. This trend can be further proven by plotting the mean fluorescence of cells as a function of DOX concentration of the NGs (Figure 16 right panel).

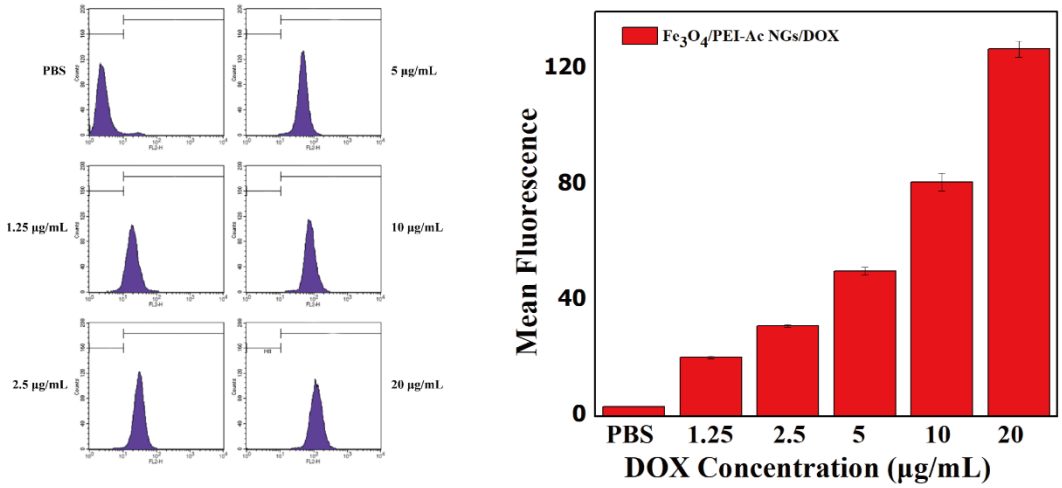

Figure 16. Flow cytometric analysis of 4T1 cells treated with Fe_3O_4/PEI-Ac NGs/DOX at different DOX concentrations for 4 h. The 4T1 cells treated with PBS were used as a control. In the right panel, the mean fluorescence of cells treated with Fe_3O_4/PEI-Ac NGs/DOX as a function of DOX concentration is shown.

To further confirm the NG uptake by cells, we examined the cellular Fe uptake by ICP-OES. After 4T1 cells were treated with the Fe_3O_4/PEI-Ac NGs/DOX at different DOX concentrations for 24 h, the 4T1 cells were digested by aqua regia and subjected to ICP-OES assay (**Figure 17**). Obviously, the cellular Fe uptake of Fe_3O_4/PEI-Ac NGs /DOX increases with the increase of the concentration of DOX, which is consistent with the results obtained from confocal laser scanning microscopy and flow cytometry analysis.

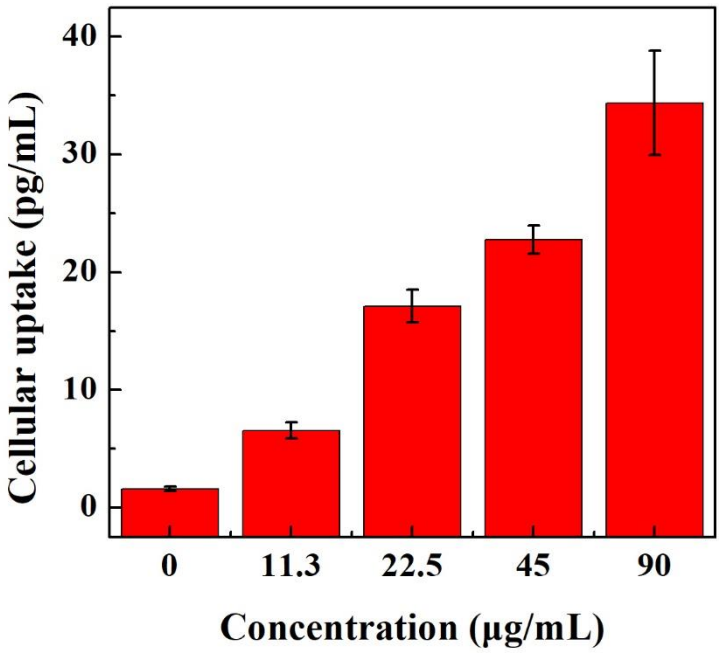

Figure 17. Fe uptake in the 4T1 cells treated with the Fe_3O_4/PEI-Ac NGs/DOX at different DOX concentrations for 24 h. The 4T1 cells treated with PBS were used as a control.

2.6 In vivo antitumor therapy and MR imaging of tumors

Antitumor effect *in vivo*. The processes of the *in vivo* treatment are shown in **Figure 18 a**. As shown in **Figure 18 b**, after drug administration for 30 days, the survival rate of PBS and drug-free Fe_3O_4/PEI-Ac NGs groups was only 40%, while those of free DOX group and Fe_3O_4/PEI-Ac NGs/DOX group were 60% and 80%, respectively. Accordingly, the survival time of mice in the free DOX group and Fe_3O_4/PEI-Ac NGs/DOX group could be prolonged. In **Figure 18c**, both groups of free DOX and Fe_3O_4/PEI-Ac NGs/DOX (treatment group) have a relatively small tumor volume change, and the Fe_3O_4/PEI-Ac NGs/DOX group has a better tumor inhibition effect than free DOX group. On the contrary, the drug-free Fe_3O_4/PEI-Ac NGs group exhibits the same tumor growth trend as the PBS. In any case, the 4 groups show the same body weight change with slightly increasing trend after 15 days of treatment (as shown in Figure 18d). This means that all the treatments do not exert systemic toxicity to the tumor-bearing mice.

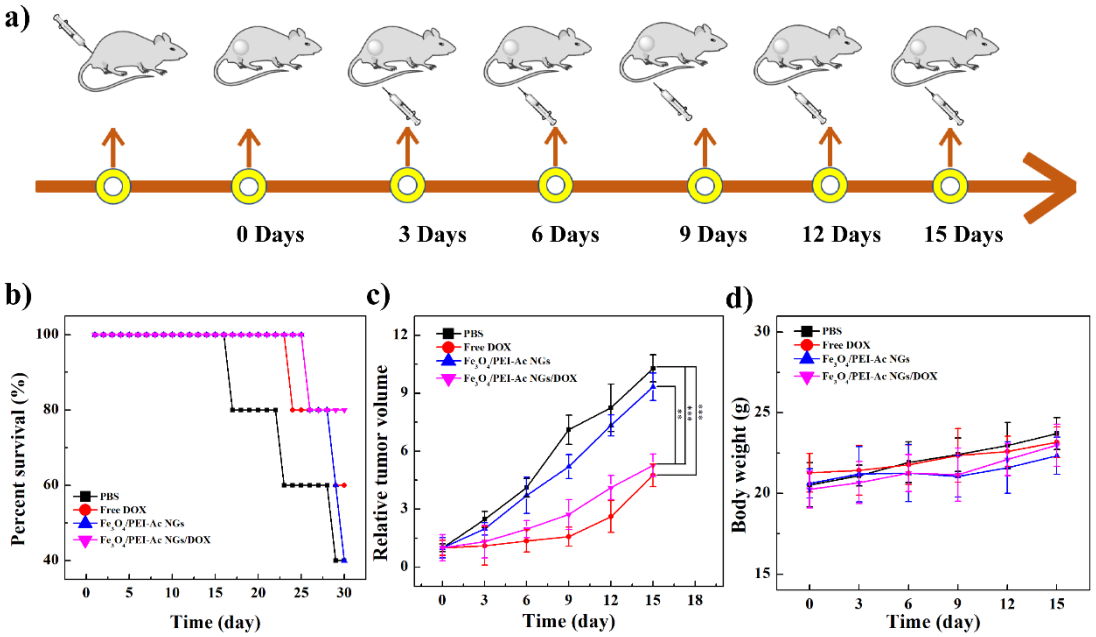

Figure 18. Antitumor therapy *in vivo*. (a) Schematic diagram of the treatment process of the tumor-bearing mice *in vivo*. (b) Survival rate of the mice in each group during 30 days treatment. (c) Relative tumor volume and (d) Body weight of mice after different treatments for 15 days.

Biodistribution of Fe element. We measured the Fe distribution of the NGs in major organs and tumor at different time points post administration. As shown in **Figure 19**, Fe_3O_4/PEI-Ac NGs/DOX are mainly cleared by spleen, lung and kidney. The Fe content

dramatically increases in these organs after administration and rises to the maximum at 1 h post injection. Then the Fe content decreases gradually. After 48 h of administration, the Fe content material in each major organ was very small. This indicates that the Fe_3O_4/PEI-Ac NGs/DOX can be gradually metabolized *in vivo* and have good *in vivo* biocompatibility.

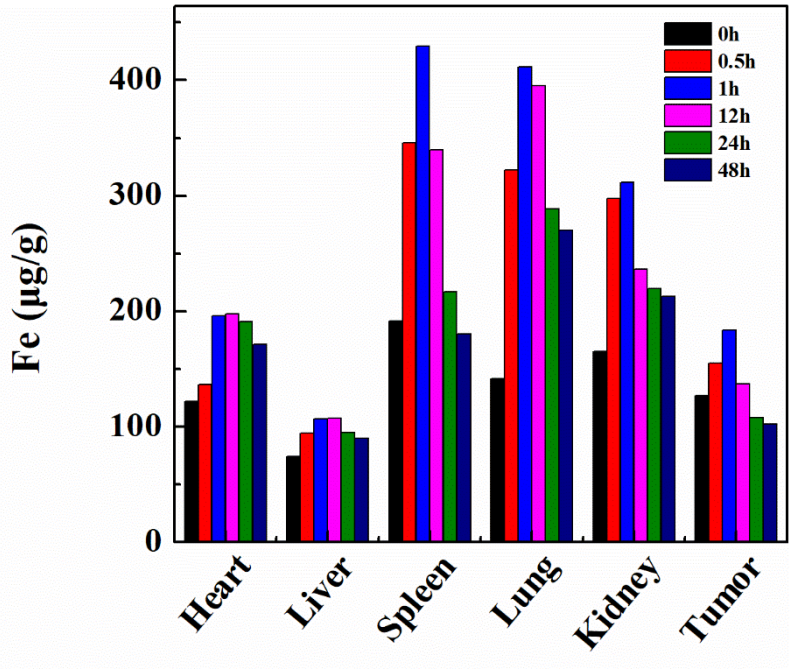

Figure 19. The Fe biodistribution in major organs and tumor of the mice at different time points post injection of the Fe_3O_4/PEI-Ac NGs/DOX (Fe mass = 150 μg, in 0.2 mL PBS for each mouse).

H&E staining. As shown in **Figure 20**, the injection of the Fe_3O_4/PEI-Ac NGs/DOX does not seem to cause any significant damages to major organs of mice, and there is no significant change in organ morphology when compared with the control group. This indicates that the developed Fe_3O_4/PEI-Ac NGs/DOX do not influence the major organs of mice, thus having a good biosafety profile.

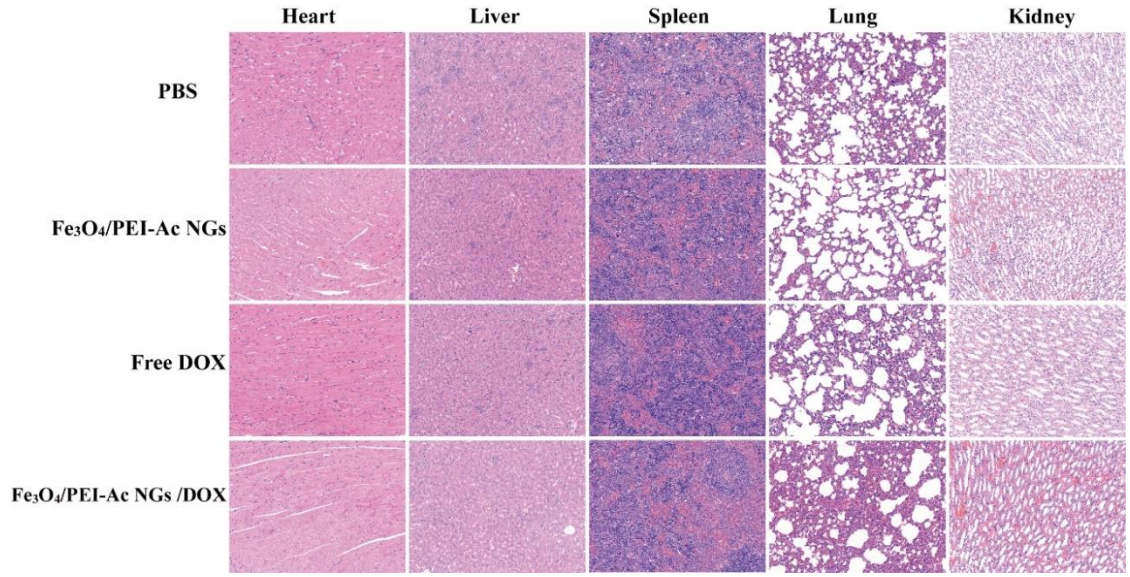

Figure 20. Representative H&E staining of the sections of the heart, liver, spleen, lung and kidney after each tumor-bearing mouse was treated with PBS, free DOX, Fe_3O_4/PEI-Ac NGs/DOX and Fe_3O_4/PEI-Ac NGs complexes for 30 days.

TUNEL staining. As shown in Figure 21, the green part represents the apoptotic cells, and the blue part represents the cell nucleus. The TUNEL staining results of free DOX and Fe_3O_4/PEI-Ac NGs/DOX groups reveal that these two materials cause massive apoptosis of tumor cells, which is significantly different from the PBS group and drug-free Fe_3O_4/PEI-Ac NGs group.

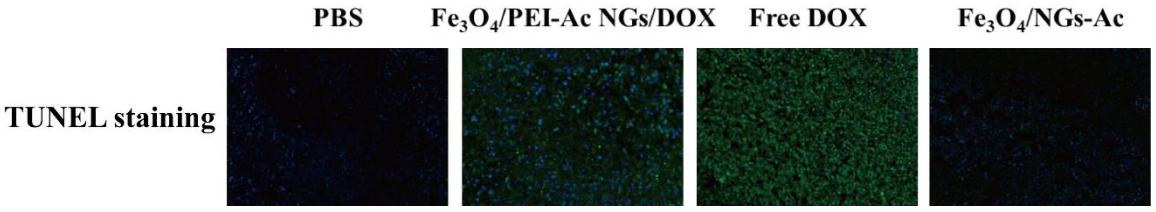

Figure 21. Representative TUNEL staining of tumor sections after the treatment with PBS, free DOX, Fe_3O_4/PEI-Ac NGs/DOX and Fe_3O_4/PEI-Ac NGs complexes, respectively for 30 days.

MR imaging of tumors. As shown in Figure 22, compared with the blank group before injection, the tumor MR signal intensity increases after the injection of the PBS solution of Fe_3O_4/PEI-Ac NGs/DOX and ultrasmall Fe_3O_4 NPs (**Figure 22 a**). This suggests that ultrasmall Fe_3O_4 NPs and Fe_3O_4/PEI-Ac NGs/DOX can be enriched and presented in the tumor site with blood circulation after intravenous injection. In particular, the injection of Fe_3O_4/PEI-Ac NGs/DOX leads to the gradual enhancement of tumor MR signal and the

tumor MR signal reaches the peak value at 30 min post injection. After 30 min, the tumor MR signal intensity slowly declines, and the MR signal can be maintained for at least 75 min. By quantitatively analyzing the MR signal to noise ratio (SNR), we show that the tumor MR SNR for the NG group is much larger than that for the ultrasmall Fe_3O_4 NP group at the same time points post injection (**Figure 22 b**). This means that the Fe_3O_4/PEI-Ac NGs/DOX display a better MR imaging performance than the ultrasmall Fe_3O_4 NPs, possibly due to the better r_1 relaxivity of the NGs.

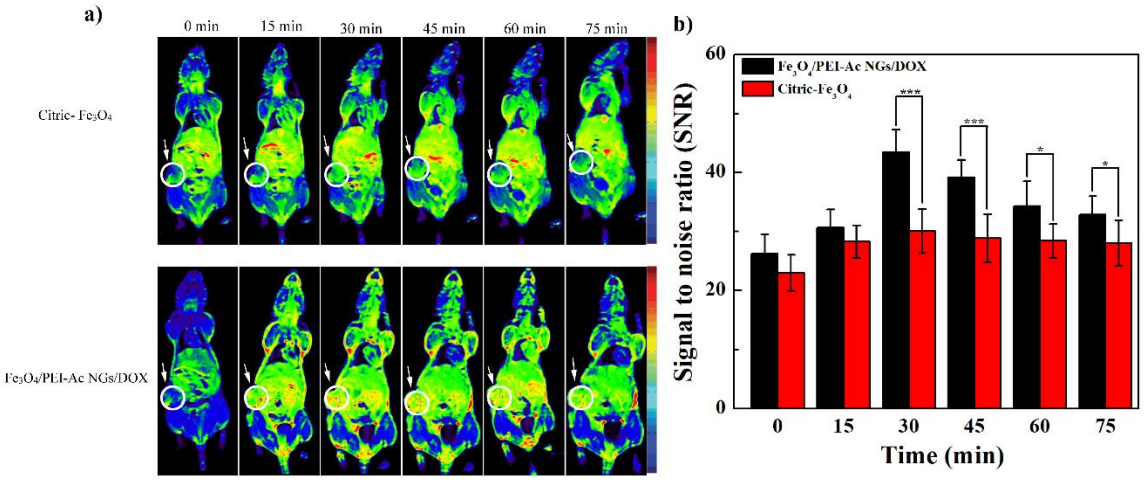

Figure 22. *In vivo* T_1-weighted MR images (a) and signal to noise ratio (b) of xenograft 4T1 tumors before and at different time points post intravenous injection of the ultrasmall Fe_3O_4 NPs or the Fe_3O_4/NGs-Ac NGs/DOX (Fe mass = 150 μg, in 0.2 mL PBS for each mouse).

CHAPTER 4 – GENERAL CONCLUSION

CHAPTER 4 – GENERAL CONCLUSIONS

In this study, we developed a unique method to generate hybrid PEI-based NGs modified with ultrasmall Fe_3O_4 NPs and loaded with anticancer drug DOX for theranostics of tumors. Through the rational design and precise synthesis of hybrid NGs, both imaging agents of ultrasmall Fe_3O_4 NPs and anticancer drug DOX can be loaded within a single PEI-based platform for MR imaging-guided chemotherapy of tumors. The hybrid NGs presented double r_1 relaxivity times when compared with ultra-small iron oxide without NGs. It is a significant improvement of the T_1 contrast agents, which is caused by the PEI-based NGs that are able to improve the dispersiveness of the ultra-small iron oxide, making them more stable and not easily aggregated. After loading with DOX, the hybrid NGs presented different release rates under different pH conditions. In the acidic environment, which has a pH value similar to the tumor organ, the hybrid NGs showed better performance. In this study, 4T1 cells and the xenografted 4T1 tumors were used as models to study the performance of the hybrid NGs. We show that the MR imaging capability of the hybrid NGs is significantly enhanced, and the tumor suppression effect of the hybrid NGs is significantly improved. Such development of hybrid NGs may be used for theranostics of different types of tumors.

REFERENCES

1. Kong, J.; Franklin, N. R.; Zhou, C.; Chapline, M. G.; Peng, S.; Cho, K.; Dai, H., Nanotube molecular wires as chemical sensors. *Science* **2000,** *287*, 622-625.
2. Gong, K.; Du, F.; Xia, Z.; Durstock, M.; Dai, L., Nitrogen-doped carbon nanotube arrays with high electrocatalytic activity for oxygen reduction. *Science* **2009,** *323*, 760-764.
3. Dreher, M. R.; Simnick, A. J.; Fischer, K.; Smith, R. J.; Patel, A.; Schmidt, M.; Chilkoti, A., Temperature triggered self-assembly of polypeptides into multivalent spherical micelles. *J. Am. Chem. Soc.* **2008,** *130*, 687-694.
4. Carey, G. H.; Abdelhady, A. L.; Ning, Z.; Thon, S. M.; Bakr, O. M.; Sargent, E. H., Colloidal quantum dot solar cells. *Chem. Rev.* **2015,** *115*, 12732-12763.
5. Swarnkar, A.; Marshall, A. R.; Sanehira, E. M.; Chernomordik, B. D.; Moore, D. T.; Christians, J. A.; Chakrabarti, T.; Luther, J. M., Quantum dot–induced phase stabilization of α-CsPbI3 perovskite for high-efficiency photovoltaics. *Science* **2016,** *354*, 92-95.
6. Zhang, K.; Zhang, L. L.; Zhao, X.; Wu, J., Graphene/polyaniline nanofiber composites as supercapacitor electrodes. *Chem. Mater.* **2010,** *22*, 1392-1401.
7. Sasaki, Y.; Akiyoshi, K., Nanogel engineering for new nanobiomaterials: from chaperoning engineering to biomedical applications. *Chem. Rec.* **2010,** *10*, 366-376.
8. Mauri, E.; Moroni, I.; Magagnin, L.; Masi, M.; Sacchetti, A.; Rossi, F., Comparison between two different click strategies to synthesize fluorescent nanogels for therapeutic applications. *React. Funct. Polym.* **2016,** *105*, 35-44.
9. Naahidi, S.; Jafari, M.; Logan, M.; Wang, Y.; Yuan, Y.; Bae, H.; Dixon, B.; Chen, P., Biocompatibility of hydrogel-based scaffolds for tissue engineering applications. *Biotechnol. Adv.* **2017,** *35*, 530-544.
10. Liang, K.; Ng, S.; Lee, F.; Lim, J.; Chung, J. E.; Lee, S. S.; Kurisawa, M., Targeted intracellular protein delivery based on hyaluronic acid-green tea catechin nanogels. *Acta Biomater.* **2016,** *33*, 142-152.
11. Priya, M. V.; Sabitha, M.; Jayakumar, R., Colloidal chitin nanogels: A plethora of applications under one shell. *Carbohydr. Polym.* **2016,** *136*, 609-617.
12. Xue, K.; Wang, X.; Yong, P. W.; Young, D. J.; Wu, Y.-L.; Li, Z.; Loh, X. J., Hydrogels as Emerging Materials for Translational Biomedicine. *Adv. Ther.* **2019,** *2*, 1800088.
13. Vinogradov, S.; Batrakova, E.; Kabanov, A., Poly(ethylene glycol)-polyethyleneimine NanoGel (TM) particles: novel drug delivery systems for antisense oligonucleotides. *Colloids Surf., B* **1999,** *16*, 291-304.
14. McAllister, K.; Sazani, P.; Adam, M.; Cho, M. J.; Rubinstein, M.; Samulski, R. J.; DeSimone, J. M., Polymeric nanogels produced via inverse microemulsion polymerization as potential gene and antisense delivery agents. *J. Am. Chem. Soc.* **2002,** *124*, 15198-15207.
15. Vinogradov, S. V.; Zeman, A. D.; Batrakova, E. V.; Kabanov, A. V., Polyplex Nanogel formulations for drug delivery of cytotoxic nucleoside analogs. *J. Controlled Release* **2005,** *107*, 143-157.
16. Vinogradov, S. V., Colloidal microgels in drug delivery applications. *Curr. Pharm. Des.* **2006,** *12*, 4703-4712.
17. Raemdonck, K.; Demeester, J.; De Smedt, S., Advanced nanogel engineering for drug delivery. *Soft Matter* **2009,** *5*, 707-715.
18. Gui, R.; An, X.; Gong, J.; Chen, T., Thermosensitive, reversible luminescence properties and bright fluorescence imaging of water-soluble quantum dots/microgels nanocompounds. *Mater. Lett.* **2012,** *88*, 122-125.
19. Sun, W.; Zhang, J.; Zhang, C.; Zhou, Y.; Zhu, J.; Peng, C.; Shen, M.; Shi, X., A unique nanogel-based platform for enhanced dual mode tumor MR/CT imaging. *J. Mater. Chem. B*

2018, *6*, 4835-4842.
20. Steinhilber, D.; Witting, M.; Zhang, X.; Staegemann, M.; Paulus, F.; Friess, W.; Küchler, S.; Haag, R., Surfactant free preparation of biodegradable dendritic polyglycerol nanogels by inverse nanoprecipitation for encapsulation and release of pharmaceutical biomacromolecules. *J. Controlled Release* **2013,** *169*, 289-295.
21. Nagahama, K.; Sano, Y.; Kumano, T., Anticancer drug-based multifunctional nanogels through self-assembly of dextran-curcumin conjugates toward cancer theranostics. *Bioorg. Med. Chem. Lett.* **2015,** *25*, 2519-2522.
22. Deng, Z.; Xiao, Y.; Pan, M.; Li, F.; Duan, W.; Meng, L.; Liu, X.; Yan, F.; Zheng, H., Hyperthermia-triggered drug delivery from iRGD-modified temperature-sensitive liposomes enhances the anti-tumor efficacy using high intensity focused ultrasound. *J. Controlled Release* **2016,** *243*, 333-341.
23. Liu, J.; Yang, G.; Zhu, W.; Dong, Z.; Yang, Y.; Chao, Y.; Liu, Z., Light-controlled drug release from singlet-oxygen sensitive nanoscale coordination polymers enabling cancer combination therapy. *Biomaterials* **2017,** *146*, 40-48.
24. Li, Y.; Maciel, D.; Rodrigues, J.; Shi, X.; Tomás, H., Biodegradable Polymer Nanogels for Drug/Nucleic Acid Delivery. *Chem. Rev.* **2015,** *115*, 8564-8608.
25. Ratanajanchai, M.; Soodvilai, S.; Pimpha, N.; Sunintaboon, P., Polyethylenimine-immobilized core–shell nanoparticles: Synthesis, characterization, and biocompatibility test. *Mater. Sci. Eng., C* **2014,** *34*, 377-383.
26. Sahiner, N.; Demirci, S.; Sahiner, M.; Al-Lohedan, H., The synthesis of desired functional groups on PEI microgel particles for biomedical and environmental applications. *Appl. Surf. Sci.* **2015,** *354*, 380-387.
27. Li, H.; Yang, X.; Gao, F.; Qian, C.; Li, C.; Oupicky, D.; Sun, M., Bioreduction-ruptured nanogel for switch on/off release of Bcl2 siRNA in breast tumor therapy. *J. Controlled Release* **2018,** *292*, 78-90.
28. Sahiner, N., Preparation of poly (ethylene imine) particles for versatile applications. *Colloids Surf., A* **2013,** *433*, 212-218.
29. Sahiner, N.; Demirci, S., Can PEI microgels become biocompatible upon betainization? *Mater. Sci. Eng., C* **2017,** *77*, 642-648.
30. Akiyoshi, K.; Deguchi, S.; Tajima, H.; Nishikawa, T.; Sunamoto, J., Microscopic structure and thermoresponsiveness of a hydrogel nanoparticle by self-assembly of a hydrophobized polysaccharide. *Macromolecules* **1997,** *30*, 857-861.
31. Jiang, Y.; Chen, J.; Deng, C.; Suuronen, E. J.; Zhong, Z., Click hydrogels, microgels and nanogels: emerging platforms for drug delivery and tissue engineering. *Biomaterials* **2014,** *35*, 4969-4985.
32. Schubert, S.; Delaney Jr, J. T.; Schubert, U. S., Nanoprecipitation and nanoformulation of polymers: from history to powerful possibilities beyond poly (lactic acid). *Soft Matter* **2011,** *7*, 1581-1588.
33. Sahiner, N.; Sagbas, S.; Sahiner, M.; Demirci, S., Degradable tannic acid/polyethyleneimine polyplex particles with highly antioxidant and antimicrobial effects. *Polym. Degrad. Stab.* **2016,** *133*, 152-161.
34. Peng, H.; Ruebsam, K.; Jakob, F.; Schwaneberg, U.; Pich, A., Tunable Enzymatic Activity and Enhanced Stability of Cellulase Immobilized in Biohybrid Nanogels. *Biomacromolecules* **2016,** *17*, 3619-3631.
35. Sun, W.; Yang, J.; Zhu, J.; Zhou, Y.; Li, J.; Zhu, X.; Shen, M.; Zhang, G.; Shi, X., Immobilization of iron oxide nanoparticles within alginate nanogels for enhanced MR imaging applications. *Biomater. Sci.* **2016,** *4*, 1422-30.
36. Hennink, W. E.; Nostrum, C. F. V., Novel crosslinking methods to design hydrogels *Adv. Drug Delivery Rev.* **2012,** *64*, 223-236.

37. Zhu, J.; Peng, C.; Sun, W.; Yu, Z.; Zhou, B.; Li, D.; Luo, Y.; Ding, L.; Shen, M.; Shi, X., Formation of iron oxide nanoparticle-loaded γ-polyglutamic acid nanogels for MR imaging of tumors. *J. Mater. Chem. B* **2015,** *3*, 8684-8693.
38. Gou, M.; Men, K.; Zhang, J.; Li, Y.; Song, J.; Luo, S.; Shi, H.; Wen, Y.; Guo, G.; Huang, M.; Zhao, X.; Qian, Z.; Wei, Y., Efficient Inhibition of C-26 Colon Carcinoma by VSVMP Gene Delivered by Biodegradable Cationic Nanogel Derived from Polyethyleneimine. *Acs Nano* **2010,** *4*, 5573-5584.
39. Dey, D.; Inayathullah, M.; Lee, A. S.; LeMieux, M. C.; Zhang, X.; Wu, Y.; Nag, D.; De Almeida, P. E.; Han, L.; Rajadas, J.; Wu, J. C., Efficient gene delivery of primary human cells using peptide linked polyethylenimine polymer hybrid. *Biomaterials* **2011,** *32*, 4647-4658.
40. Dimde, M.; Neumann, F.; Reisbeck, F.; Ehrmann, S.; Cuellar-Camacho, J. L.; Steinhilber, D.; Ma, N.; Haag, R., Defined pH-sensitive nanogels as gene delivery platform for siRNA mediated in vitro gene silencing. *Biomater. Sci.* **2017,** *5*, 2328-2336.
41. Park, J. S.; Yi, S. W.; Kim, H. J.; Park, K.-H., Receptor-mediated gene delivery into human mesenchymal stem cells using hyaluronic acid-shielded polyethylenimine/pDNA nanogels. *Carbohydr. Polym.* **2016,** *136*, 791-802.
42. Costa, D.; Valente, A. J. M.; Queiroz, J., Stimuli-responsive polyamine-DNA blend nanogels for co-delivery in cancer therapy. *Colloids Surf., B* **2015,** *132*, 194-201.
43. Wang, K.; Mao, W.; Sui, M.; Tang, J.; Shen, Y., Biodegradable charge-reversal PEI derivative for gene transfection. *J. Controlled Release* **2013,** *172*, E109-E110.
44. Li, P.; Luo, Z.; Liu, P.; Gao, N.; Zhang, Y.; Pan, H.; Liu, L.; Wang, C.; Cai, L.; Ma, Y., Bioreducible alginate-poly(ethylenimine) nanogels as an antigen-delivery system robustly enhance vaccine-elicited humoral and cellular immune responses. *J. Controlled Release* **2013,** *168*, 271-279.
45. Hong, C. A.; Kim, J. S.; Lee, S. H.; Kong, W. H.; Park, T. G.; Mok, H.; Nam, Y. S., Reductively Dissociable siRNA-Polymer Hybrid Nanogels for Efficient Targeted Gene Silencing. *Adv. Funct. Mater.* **2013,** *23*, 316-322.
46. Kim, C.; Lee, Y.; Lee, S. H.; Kim, J. S.; Jeong, J. H.; Park, T. G., Self-Crosslinked Polyethylenimine Nanogels for Enhanced Intracellular Delivery of siRNA. *Macromol. Res.* **2011,** *19*, 166-171.
47. Ambardekar, V. V.; Han, H.-Y.; Varney, M. L.; Vinogradov, S. V.; Singh, R. K.; Vetro, J. A., The modification of siRNA with 3 ' cholesterol to increase nuclease protection and suppression of native mRNA by select siRNA polyplexes. *Biomaterials* **2011,** *32*, 1404-1411.
48. Khondee, S.; Yakovleva, T.; Berkland, C., Low Charge Polyvinylamine Nanogels Offer Sustained, Low-Level Gene Expression. *J. Appl. Polym. Sci.* **2010,** *118*, 1921-1932.
49. Dong, L.; Xu, H.; Liu, Y. B.; Lu, B.; Xu, D. M.; Li, B. H.; Gao, J.; Wu, M.; Yao, S. D.; Zhao, J.; Guo, Y. J., M-PEIs nanogels: potential nonviral vector for systemic plasmid delivery to tumor cells. *Cancer Gene Ther.* **2009,** *16*, 561-566.
50. Li, L.; Tong, J.; Wu, J.; Du, J.; Wang, J., Synthesis and characterization of polyethylenimine-poly(ethylene glycol) diacrylate nanogel as a siRNA carrier. *Acta Polym. Sin.* **2009**, 257-263.
51. Cheng, H.; Li, Y.-Y.; Zeng, X.; Sun, Y.-X.; Zhang, X.-Z.; Zhuo, R.-X., Protamine sulfate/poly(L-aspartic acid) polyionic complexes self-assembled via electrostatic attractions for combined delivery of drug and gene. *Biomaterials* **2009,** *30*, 1246-1253.
52. Yao, Y.-H.; Liu, Y.-B.; Feng, Y.; Feng, X.; Xu, D.-M.; Yao, S.-D., Synthesis and screening of polyethylenimine as a carrier for gene transfer into cultured human tumor cells. *Chin. J. Cancer* **2007,** *26*, 790-4.
53. Xu, D.-M.; Yao, S.-D.; Liu, Y.-B.; Sheng, K.-L.; Hong, J.; Gong, P.-J.; Dong, L., Size-dependent properties of M-PEIs nanogels for gene delivery in cancer cells. *Int. J. Pharm.* **2007,** *338*, 291-296.

54. Oishi, M.; Hayashi, H.; Itaka, K.; Kataoka, K.; Nagasaki, Y., pH-responsive PEGylated nanogels as targetable and low invasive endosomolytic agents to induce the enhanced transfection efficiency of nonviral gene vectors. *Colloid Polym. Sci.* **2007,** *285*, 1055-1060.
55. Xu, D.; Yu, J.; Liu, Y.; Sun, H.; Xu, J.; Sheng, K.; Yao, S.; Xu, Y.; Lu, H., *Novel polyethylenimine nanogels as potential gene carriers produced via photochemistry in surfactant-free aqueous solution*. 2006; Vol. 5, p 753-+.
56. Xu, D.; Yu, J.; Liu, Y.; Sun, H.; Gong, P.; Hong, J.; Yao, S., Photochemistry synthesis of PEI for gene delivery with high transfection efficiency. *J. Radiat. Res. Radiat. Process.* **2005,** *23*, 81-81.
57. Zhang, L.; Wang, Y.; Jin, C.; Dong, X.; Li, W., In vitro anti-tumor effect of RRM2-siRNA based on active and passive dual targeted nanogel. *Acad. J. Second Mil. Med. Univ.* **2017,** *38*, 720-726.
58. Lemieux, P.; Vinogradov, S. V.; Gebhart, C. L.; Guerin, N.; Paradis, G.; Nguyen, H. K.; Ochietti, B.; Suzdaltseva, Y. G.; Bartakova, E. V.; Bronich, T. K.; St-Pierre, Y.; Alakhov, V. Y.; Kabanov, A. V., Block and graft copolymers and Nanogel (TM) copolymer networks for DNA delivery into cell. *J. Drug Targeting* **2000,** *8*, 91-105.
59. Zhou, X.; Li, X.; Gou, M.; Qiu, J.; Li, J.; Yu, C.; Zhang, Y.; Zhang, N.; Teng, X.; Chen, Z.; Luo, C.; Wang, Z.; Liu, X.; Shen, G.; Yang, L.; Qian, Z.; Wei, Y.; Li, J., Antitumoral efficacy by systemic delivery of heparin conjugated polyethylenimine-plasmid interleukin-15 complexes in murine models of lung metastasis. *Cancer Sci.* **2011,** *102*, 1403-1409.
60. Liu, P.; Gou, M.; Yi, T.; Qi, X.; Xie, C.; Zhou, S.; Deng, H.; Wei, Y.; Zhao, X., The enhanced antitumor effects of biodegradable cationic heparin-polyethyleneimine nanogels delivering HSulf-1 gene combined with cisplatin on ovarian cancer. *Int. J. Oncol.* **2012,** *41*, 1504-1512.
61. Liu, P.; Gou, M.; Yi, T.; Xie, C.; Qi, X.; Zhou, S.; Deng, H.; Wei, Y.; Zhao, X., Efficient inhibition of an intraperitoneal xenograft model of human ovarian cancer by HSulf-1 gene delivered by biodegradable cationic heparin-polyethyleneimine nanogels. *Oncol. Rep.* **2012,** *27*, 363-370.
62. Song, L.; Liang, X.; Yang, S.; Wang, N.; He, T.; Wang, Y.; Zhang, L.; Wu, Q.; Gong, C., Novel polyethyleneimine-R8-heparin nanogel for high-efficiency gene delivery in vitro and in vivo. *Drug Delivery* **2018,** *25*, 122-131.
63. Boussif, O.; Lezoualc'h, F.; Zanta, M. A.; Mergny, M. D.; Scherman, D.; Demeneix, B.; Behr, J.-P., A versatile vector for gene and oligonucleotide transfer into cells in culture and in vivo: polyethylenimine. *Proc. Natl. Acad. Sci.* **1995,** *92*, 7297-7301.
64. Godbey, W.; Wu, K. K.; Mikos, A. G., Poly (ethylenimine) and its role in gene delivery. *J. Controlled Release* **1999,** *60*, 149-160.
65. Zabner, J.; Fasbender, A. J.; Moninger, T.; Poellinger, K. A.; Welsh, M. J., Cellular and molecular barriers to gene transfer by a cationic lipid. *J. Biol. Chem.* **1995,** *270*, 18997-19007.
66. Liu, X.; Xiang, J.; Zhu, D.; Jiang, L.; Zhou, Z.; Tang, J.; Liu, X.; Huang, Y.; Shen, Y., Fusogenic reactive oxygen species triggered charge-reversal vector for effective gene delivery. *Adv. Mater.* **2016,** *28*, 1743-1752.
67. Hölttä-Vuori, M.; Ikonen, E., Endosomal cholesterol traffic: vesicular and non-vesicular mechanisms meet. Portland Press Limited: 2006.
68. Goldberg, M.; Langer, R.; Jia, X., Nanostructured materials for applications in drug delivery and tissue engineering. *J. Biomater. Sci., Polym. Ed.* **2007,** *18*, 241-268.
69. Vinogradov, S. V.; Batrakova, E. V.; Kabanov, A. V., Nanogels for oligonucleotide delivery to the brain. *Bioconjugate Chem.* **2004,** *15*, 50-60.
70. Kabanov, A. V.; Vinogradov, S. V., Nanogels as pharmaceutical carriers: finite networks of infinite capabilities. *Angew. Chem. Int. Ed. Engl.* **2009,** *48*, 5418-29.
71. Vinogradov, S. V.; Kohli, E.; Zeman, A. D., Comparison of nanogel drug carriers and

their formulations with nucleoside 5 '-triphosphates. *Pharm. Res.* **2006,** *23*, 920-930.
72. Vinogradov, S. V.; Kohli, E.; Zeman, A. D., Cross-linked polymeric nanogel formulations of 5 '-triphosphates of nucleoside analogues: Role of the cellular membrane in drug release. *Mol. Pharmaceutics* **2005,** *2*, 449-461.
73. Li, N.; Wang, J.; Yang, X.; Li, L., Novel nanogels as drug delivery systems for poorly soluble anticancer drugs. *Colloids Surf., B* **2011,** *83*, 237-244.
74. Wu, S.-Y.; Debele, T. A.; Kao, Y.-C.; Tsai, H.-C., Synthesis and Characterization of Dual-Sensitive Fluorescent Nanogels for Enhancing Drug Delivery and Tracking Intracellular Drug Delivery. *Int. J. Mol. Sci.* **2017,** *18*.
75. Qiao, Z.; Shi, X., Dendrimer-based molecular imaging contrast agents. *Prog. Polym. Sci.* **2015,** *44*, 1-27.
76. Hu, Y.; Mignani, S.; Majoral, J.-P.; Shen, M.; Shi, X., Construction of iron oxide nanoparticle-based hybrid platforms for tumor imaging and therapy. *Chem. Soc. Rev.* **2018,** *47*, 1874-1900.
77. Yang, H.; Zhang, C.; Shi, X.; Hu, H.; Du, X.; Fang, Y.; Ma, Y.; Wu, H.; Yang, S., Water-soluble superparamagnetic manganese ferrite nanoparticles for magnetic resonance imaging. *Biomaterials* **2010,** *31*, 3667-3673.
78. Li, J.; He, Y.; Sun, W.; Luo, Y.; Cai, H.; Pan, Y.; Shen, M.; Xia, J.; Shi, X., Hyaluronic acid-modified hydrothermally synthesized iron oxide nanoparticles for targeted tumor MR imaging. *Biomaterials* **2014,** *35*, 3666-3677.
79. Yang, H.; Zhuang, Y.; Hu, H.; Du, X.; Zhang, C.; Shi, X.; Wu, H.; Yang, S., Silica-coated manganese oxide nanoparticles as a platform for targeted magnetic resonance and fluorescence imaging of cancer cells. *Adv. Funct. Mater.* **2010,** *20*, 1733-1741.
80. Liu, H.; Xu, Y.; Wen, S.; Chen, Q.; Zheng, L.; Shen, M.; Zhao, J.; Zhang, G.; Shi, X., Targeted tumor computed tomography imaging using low-generation dendrimer-stabilized gold nanoparticles. *Chem. - Eur. J.* **2013,** *19*, 6409-6416.
81. Liu, H.; Wang, H.; Xu, Y.; Shen, M.; Zhao, J.; Zhang, G.; Shi, X., Synthesis of PEGylated low generation dendrimer-entrapped gold nanoparticles for CT imaging applications. *Nanoscale* **2014,** *6*, 4521-4526.
82. Cai, H.; Li, K.; Li, J.; Wen, S.; Chen, Q.; Shen, M.; Zheng, L.; Zhang, G.; Shi, X., Dendrimer-assisted formation of Fe3O4/Au nanocomposite particles for targeted dual mode CT/MR imaging of tumors. *Small* **2015,** *11*, 4584-4593.
83. Yang, J.; Luo, Y.; Xu, Y.; Li, J.; Zhang, Z.; Wang, H.; Shen, M.; Shi, X.; Zhang, G., Conjugation of iron oxide nanoparticles with RGD-modified dendrimers for targeted tumor MR imaging. *ACS Appl. Mater. Interfaces* **2015,** *7*, 5420-5428.
84. Ogawa, M.; Regino, C. A. S.; Seidel, J., Dual-Modality Molecular Imaging Using Antibodies Labeled with Activatable Fluorescence and a Radionuclide for Specific and Quantitative Targeted Cancer Detection. *Bioconjugate Chem.* **2009,** *20*, 2177-2184.
85. Li, X.; Xing, L.; Zheng, K.; Wei, P.; Du, L.; Shen, M.; Shi, X., Formation of gold nanostar-coated hollow mesoporous silica for tumor multimodality imaging and photothermal therapy. *ACS Appl. Mater. Interfaces* **2017,** *9*, 5817-5827.
86. Zhu, J.; Zhao, L.; Cheng, Y.; Xiong, Z.; Tang, Y.; Shen, M.; Zhao, J.; Shi, X., Radionuclide 131 I-labeled multifunctional dendrimers for targeted SPECT imaging and radiotherapy of tumors. *Nanoscale* **2015,** *7*, 18169-18178.
87. Li, X.; Xiong, Z.; Xu, X.; Luo, Y.; Peng, C.; Shen, M.; Shi, X., 99mTc-labeled multifunctional low-generation dendrimer-entrapped gold nanoparticles for targeted SPECT/CT dual-mode imaging of tumors. *ACS Appl. Mater. Interfaces* **2016,** *8*, 19883-19891.
88. Cheng, D.; Wang, Y.; Liu, X.; Pretorius, P. H.; Liang, M.; Rusckowski, M.; Hnatowich, D. J., A comparison of 18F PET and 99mTc SPECT imaging in phantoms and in tumored mice. *Bioconjugate Chem.* **2010,** *21*, 1565-1570.

89. Cheng, L.; Liu, J.; Gu, X.; Gong, H.; Shi, X.; Liu, T.; Wang, C.; Wang, X.; Liu, G.; Xing, H., PEGylated WS2 nanosheets as a multifunctional theranostic agent for in vivo dual-modal CT/photoacoustic imaging guided photothermal therapy. *Adv. Mater.* **2014,** *26*, 1886-1893.
90. Zhou, Y.; Hu, Y.; Sun, W.; Zhou, B.; Zhu, J.; Peng, C.; Shen, M.; Shi, X., Polyaniline-loaded γ-polyglutamic acid nanogels as a platform for photoacoustic imaging-guided tumor photothermal therapy. *Nanoscale* **2017,** *9*, 12746-12754.
91. Yamashita, T.; Kitao, A.; Matsui, O.; Hayashi, T.; Nio, K.; Kondo, M.; Ohno, N.; Miyati, T.; Okada, H.; Yamashita, T., Gd-EOB-DTPA-enhanced magnetic resonance imaging and alpha-fetoprotein predict prognosis of early-stage hepatocellular carcinoma. *Hepatology* **2014,** *60*, 1674-1685.
92. Chen, H.; Wang, G. D.; Tang, W.; Todd, T.; Zhen, Z.; Tsang, C.; Hekmatyar, K.; Cowger, T.; Hubbard, R. B.; Zhang, W., Gd-encapsulated carbonaceous dots with efficient renal clearance for magnetic resonance imaging. *Adv. Mater.* **2014,** *26*, 6761-6766.
93. Lev, M. H.; Segal, A. Z.; Farkas, J.; Hossain, S. T.; Putman, C.; Hunter, G. J.; Budzik, R.; Harris, G. J.; Buonanno, F. S.; Ezzeddine, M. A., Utility of perfusion-weighted CT imaging in acute middle cerebral artery stroke treated with intra-arterial thrombolysis. *Stroke* **2001,** *32*, 2021-2028.
94. Zhuang, H.; Pourdehnad, M.; Lambright, E. S.; Yamamoto, A. J.; Lanuti, M.; Li, P.; Mozley, P. D.; Rossman, M. D.; Albelda, S. M.; Alavi, A., Dual time point 18F-FDG PET imaging for differentiating malignant from inflammatory processes. *J. Nucl. Med.* **2001,** *42*, 1412-1417.
95. Chen, W.; Silverman, D. H.; Delaloye, S.; Czernin, J.; Kamdar, N.; Pope, W.; Satyamurthy, N.; Schiepers, C.; Cloughesy, T., 18F-FDOPA PET imaging of brain tumors: comparison study with 18F-FDG PET and evaluation of diagnostic accuracy. *J. Nucl. Med.* **2006,** *47*, 904-911.
96. Zhu, J.; Sun, W.; Zhang, J.; Zhou, Y.; Shen, M.; Peng, C.; Shi, X., Facile Formation of Gold-Nanoparticle-Loaded gamma-Polyglutamic Acid Nanogels for Tumor Computed Tomography Imaging. *Bioconjugate Chem.* **2017,** *28*, 2692-2697.
97. Sun, W.; Zhang, J.; Zhang, C.; Wang, P.; Peng, C.; Shen, M.; Shi, X., Construction of Hybrid Alginate Nanogels Loaded with Manganese Oxide Nanoparticles for Enhanced Tumor Magnetic Resonance Imaging. *ACS Macro Lett.* **2018,** *7*, 137-142.
98. Lim, C. K.; Singh, A.; Heo, J.; Kim, D.; Lee, K. E.; Jeon, H.; Koh, J.; Kwon, I. C.; Kim, S., Gadolinium-coordinated elastic nanogels for in vivo tumor targeting and imaging. *Biomaterials* **2013,** *34*, 6846-52.
99. Roca, A. G.; Marco, J. F.; Morales, M. D. P.; Serna, C. J., Effect of Nature and Particle Size on Properties of Uniform Magnetite and Maghemite Nanoparticles. *J. Phys. Chem. C* **2007,** *111*, 18577-18584.

CQM
CENTRO DE QUÍMICA DA MADEIRA
UNIVERSIDADE da MADEIRA
FCT Fundação para a Ciência e a Tecnologia
MINISTÉRIO DA CIÊNCIA, TECNOLOGIA E ENSINO SUPERIOR
PEst-OE/QUI/UI0674/2019
MADEIRA 14-20
Project M1420-01-0145-FEDER-000005-CQM+